Journal of Sound and Vibration 330 (2011) 6153–6183

Contents lists available at ScienceDirect

Journal of Sound and Vibration

journal homepage: www.elsevier.com/locate/jsvi

Broadband noise prediction of fan outlet guide vane using a cascade response function

H. Posson [a,*], S. Moreau [a], M. Roger [b]

[a] GAUS, Département de Génie Mécanique, Université de Sherbrooke, 2500 Bd. de l'université, Sherbrooke, QC, Canada J1H4X2
[b] Laboratoire de Mécanique des Fluides et d'Acoustique, École Centrale de Lyon, 36 Av. Guy de Colongue, 69131 Écully Cedex, France

ARTICLE INFO

Article history:
Received 27 August 2010
Received in revised form
5 July 2011
Accepted 29 July 2011
Handling Editor: P. Joseph
Available online 15 August 2011

ABSTRACT

An analytical model of the broadband noise produced by both the interaction of ingested turbulence with a fan rotor blades and the rotor-wake impingement on downstream stator vanes is proposed and detailed. The noise prediction methodology is a strip-theory approach based on a previously published formulation of the three-dimensional unsteady blade loading for a rectilinear cascade. This three-dimensional cascade response applied in each strip combined with an acoustic analogy in an annular duct have been chosen to account for the main three-dimensional effects. To further improve some of the identified limitations of this approach, a correction is added to mitigate the effects of the non-coincidence of the cut-on frequencies of the annular duct modes and of the modes of the rectilinear cascade. A correction of the unsteady blade loading formulation, previously developed in a tonal configuration, is also introduced to account for the dispersion relation of annular duct modes in the rectilinear-cascade model. The model is compared with experimental results of the 22-in source diagnostic test (SDT) fan rig of the NASA Glenn Research Center. A numerical assessment of the simplifications proposed in the model and of the convergence of the truncated sums in spanwise wavenumbers and azimuthal orders of the incident perturbation is carried out. The subcritical gusts are shown to have a crucial effect at low frequencies, whereas they become negligible at higher frequencies. Furthermore, alternative high-frequency formulations lead to a satisfactory accuracy above a Helmholtz number based on the duct radius of 20. The strong reduction in computational time associated with these formulations could justify their use for parametric studies in industrial context. The effect of the turbulence model is also investigated showing the relevance of Liepmann's isotropic model in the SDT case, and a possible strong effect of anisotropy in static tests. Finally, the model is compared with NASA's experimental results for two outlet guide vanes at approach condition, showing a very good agreement upstream, whereas an underestimate of 3–5 dB is observed downstream in the middle frequency range.

* Corresponding author. Present address: Hélène Posson, DAMTP, Centre for Mathematical Sciences, Wilberforce Road, Cambridge CB3 0WA, United Kingdom. Tel.: +44 1223 760450.
E-mail addresses: H.Posson@damtp.cam.ac.uk, helene.posson@gmail.com (H. Posson), stephane.moreau@usherbrooke.ca (S. Moreau), michel.roger@ec-lyon.fr (M. Roger).

0022-460X/$ - see front matter © 2011 Elsevier Ltd. All rights reserved.
doi:10.1016/j.jsv.2011.07.040

Nomenclature

Latin characters

B_R number of rotor blades
B_S number of stator vanes
c blade chord length in cascade reference frame (m)
$c_d = c/\cos\varphi_I$ blade chord length at constant radius (m)
c_0 speed of sound ($m\,s^{-1}$)
d chordwise non-overlap length (stagger distance) in the cascade reference frame $\mathcal{R}_c$ (m)
$E[\cdot]$ expected value of the enclosed quantity
$E_{m,\mu}$ duct eigenfunction of the mode (m,μ)
$\mathbf{e}_{x_d}$ unit vector in the axial direction of the duct
f frequency (Hz)
g_I inter-blade distance in the duct azimuthal direction (m)
$G_d(\mathbf{x}_d,t|\mathbf{x}_{d0},t_0)$ Green's function tailored to the annular duct in uniform axial mean flow $\underline{U_{x_d}}$ for a source in $\mathbf{x}_{d0}$ at time t_0 and a receiver in $\mathbf{x}_d$ at time t.
h inter-blade distance normal to the blades in the cascade reference frame $\mathcal{R}_c$ (m)
$H_m^{(n)}(x)$ Hankel function of kind n of order m
$H_m^{(n)\prime}(x)$ Hankel function of kind n of order m derivative
j current index of the blades
$J_m(x)$, $Y_m(x)$ Bessel function of first and second kind of order m
$k_0 = \omega/c_0$ acoustic wavenumber (m^{-1})
$k^{\pm}_{x_d,m\mu}$ axial wavenumber of the duct mode (m,μ) in the duct reference frame (m^{-1})
$k^{\pm}_{x_{cd},m\mu}(r)$ axial wavenumber of the duct mode (m,μ) in the cascade reference frame, $\mathcal{R}_{cd}$, before the rotation of sweep angle (m^{-1})
$\mathbf{K}_c = (k_{x_c},k_{y_c},k_{z_c})$ current wavenumber vector in the cascade coordinate system $\mathcal{R}_c$ (m^{-1})
$\mathbf{K}_{c0} = (k_{x_{c0}},k_{y_{c0}},k_{z_{c0}})$ wavenumber vector of the incident gust in the cascade coordinate system $\mathcal{R}_c$ (m^{-1})
$\mathbf{K}_I$ current wavenumber vector in the reference frame $\mathcal{R}_I$ (m^{-1})
$(k_{x_I},k_{z_{I0}})$ current axial and radial wavenumber in the reference frame $\mathcal{R}_I$ (m^{-1})
$\mathbf{K}_{I0}$ wavenumber vector of the incident gust in the reference frame $\mathcal{R}_I$, $(I = R \text{ or } S)$ (m^{-1})
$(k_{x_{I0}},k_{z_{I0}})$ axial and radial wavenumber of the incident gust in the reference frame $\mathcal{R}_I$ (m^{-1})
l_a, l_t integral length scales of turbulence in the direction $\boldsymbol{\lambda}$ and in its normal plane (m)
L_r distance such that $S^{(j,j')}_{\mathrm{FF},cd}(x_{cd},r,\omega;x'_{cd},r',\omega)\to 0$ when $|r-r'| > L_r$ and that the cascade geometry and the flow properties can be considered unchanged over $l_r = 2L_r$ (m)
l_r radial correlation length of the unsteady blade loading, assimilated to the radial correlation length of the incident, locally homogeneous turbulence (m)
L_w width of the wakes
$M = U_c/c_0$ chordwise Mach number in the cascade reference frame $\mathcal{R}_c$
$M_{x_d} = \underline{U_{x_d}}/c_0$ duct axial Mach number
m azimuthal order of an acoustic duct mode
m_g azimuthal order of the incident gust
$\mathbf{n}$ unit outward-normal vector
$p^{\pm}(\mathbf{x}_d,t)$ acoustic pressure at point $\mathbf{x}_d$, at time t (Pa)
p^s, p^p pressure on suction and pressure side of a blade respectively (Pa)
$\mathcal{P}^{\pm}_{m,\mu}(\omega)$ pressure amplitude of the duct mode (m,μ)
P_0 mean fluid pressure (Pa)
$\mathbf{Q}_{\check{\chi}\psi,I}$ transformation matrix from duct $\mathcal{R}_I$ to cascade reference frame $\mathcal{R}_{cd}$
$\mathbf{Q}_{\check{\chi}\psi\varphi,I}$ transformation matrix from duct $\mathcal{R}_I$ to cascade reference frame $\mathcal{R}_c$
$\mathbf{Q}_{\mathrm{inv},I} = \mathbf{Q}^{-1}_{\check{\chi}\psi\varphi,I}$ inverse transformation matrix from $\mathcal{R}_c$ to $\mathcal{R}_I$
$\mathbf{q}_I$ $\mathbf{q}_I = \mathbf{Q}_{\check{\chi}\psi\varphi,I}(2,:) = (-\sin\check{\chi}_I\cos\psi_I, \cos\check{\chi}_I\cos\psi_I, -\sin\psi_I)$
r current radius (m)
$\mathcal{R}_c$ reference frame linked to the rectilinear cascade at a radius r after rotation of the sweep angle φ_I
$\mathcal{R}_{cd}$ reference frame linked to the rectilinear cascade at a radius r before rotation of the sweep angle φ_I
$\mathcal{R}_d$ fixed frame of reference linked to the duct
$\mathrm{Re}(\cdot)$ real part
$\mathcal{R}_f$ frame of reference linked to the mean flow
R_H duct hub radius (m)
$\mathcal{R}_I$ relative frame of reference linked to the annular blade row rotating at the angular velocity Ω_I
$\mathcal{R}_{nn,i}$ cross-correlation function of the non-dimensional upwash velocity $\overline{w}_i$
R_T duct tip radius (m)
s distance between two adjacent leading-edges in the cascade reference frame $\mathcal{R}_c$ (m)
$S^{(j,j')}_{\mathrm{FF},cd}(x_{cd},r,\omega;x'_{cd},r',\omega)$ cross-spectrum of the unsteady blade loadings at point M (x_{cd},r) on blade j and at point M' (x'_{cd},r') on blade j' at angular frequencies ω and ω'
$S_{\mathrm{pp}}(\omega)$ acoustic power spectral density ($dB\,Hz^{-1}$)
t time (s)
T_0 mean static fluid temperature (K)
$\mathcal{T}_u(r) = u_{\mathrm{rms}}(r)/U_{x_d}(r)$ local turbulent intensity at radius r
$\mathbf{u}(\mathbf{x}_d,t)$ fluctuating velocity vector ($m\,s^{-1}$)
$\mathbf{U} = (U_{x_d},U_r,U_\theta)$ mean velocity vector in the reference frame $\mathcal{R}_I$ ($m\,s^{-1}$)
u_a, u_t values of the root mean square (r.m.s.) velocity components in the direction $\boldsymbol{\lambda}$ and in its normal plane ($m\,s^{-1}$)
$(U_c,0,W_c)$ mean velocity components in the cascade coordinate system ($m\,s^{-1}$)
$U_{x_d}(r)$ circumferentially averaged mean axial velocity at radius r ($m\,s^{-1}$)
$U_0 = \sqrt{U_c^2+W_c^2}$ mean flow speed (with zero angle of attack) ($m\,s^{-1}$)

U_{x_d} mean axial velocity (area-averaged) (m s^{-1})
$\overline{U_\theta}$ mean tangential velocity (m s^{-1})
$w(\mathbf{x}_d,t)$ blade upwash velocity in the duct fixed-reference frame (m s^{-1})
$\check{w}_i(\mathbf{x}_d)$ upwash velocity component of the incident gust in the frame of reference $\mathcal{R}_f$ (m s^{-1})
$\overline{w}_i(\check{\mathbf{x}}_{d,R}|\dot{r})$ stochastic non-dimensional upwash velocity ($\overline{w}_i(\check{\mathbf{x}}_{d,R}|\dot{r})=\check{w}_i(\mathbf{x}_{d,R})/w_{\mathrm{rms},i}(\dot{r})$)
$w_{\mathrm{rms},i}$ upwash r.m.s. velocity (m s^{-1})
$\check{\mathbf{x}}=\mathbf{x}/l_a$ quickly varying coordinates to describe the local homogeneity of the turbulence around a radius (m)
$\dot{\mathbf{x}}=\mathbf{x}/R_T$ slowly varying coordinates to express the slow variation of the turbulence characteristics and of the geometry from one strip to a neighboring one (m)
(x_c,y_c,z_c) Cartesian coordinates in the cascade reference frame $\mathcal{R}_c$ (origin O_c), z_c spanwise (m)
(x_{cd},y_{cd},z_{cd}) Cartesian coordinates in the cascade reference frame $\mathcal{R}_{cd}$ (origin O_{cd}) before rotation of the sweep angle φ_I, z_{cd} along the radius (m)
(x_d,y_d,z_d) Cartesian coordinates in the absolute duct reference $\mathcal{R}_d$ (origin O_d) (m)
(x_d,r_d,θ_d) cylindrical coordinates in the absolute duct reference $\mathcal{R}_d$ (origin O_d) (m)
(x_I,y_I,z_I) Cartesian coordinates in the duct reference frame rotating with the blade row I, $\mathcal{R}_I$ (origin O_I) (m)
(x_I,r_I,θ_I) cylindrical coordinates in the duct reference frame rotating with the blade row $\mathcal{R}_I$ (m)
$x_{\mathrm{LE,I}}$ axial coordinate of the leading edge taken to be 0 in $r=R_H$ (m)
$y_{\mathrm{LE,I}}$ tangential coordinate of the leading edge taken to be 0 in $r=R_H$ (m)

Greek characters

$\beta=\sqrt{1-M^2}$ compressibility parameter relative to the chordwise mean velocity U_c
β_{x_d} compressibility parameter for axial mean flow
β_w compressibility parameter relative to the spanwise mean velocity W_c
$\Gamma_{m,\mu}$ squared norm of the duct eigenfunction $E_{m,\mu}$ (m^2)
$\delta_{i,j}$ Kronecker symbol equal to 1 if $i=j$, else equal to 0
$\Delta p_c(x_c,z_c,t)$ unsteady blade loading on the blade 0 at the radius r in the cascade reference frame $\mathcal{R}_c$ (Pa)
$\Delta\widehat{P}_{c,0}(x_c,\omega|\dot{r})$ pressure jump made non-dimensional by $\rho_0 c_0 w_0$ produced by a gust of amplitude w_0, and parameters σ, $k_{z_{c0}}$ and ω, on the rectilinear cascade defined at radius r
$\Delta\widehat{P}_{cd,j}(x_{cd},\dot{r},\omega_{\mathrm{ex}})$ pressure jump at the radius r, on the blade j, for a chordwise position x_{cd} in $\mathcal{R}_{cd}$ at the angular frequency of the incident excitation ω_{ex} (Pa Hz^{-1})
ϑ deterministic envelope of the rotor wakes
$\boldsymbol{\lambda}$ direction of symmetry of the axisymmetric turbulence model
Λ turbulence integral length scale for an isotropic turbulence model ($l_a=l_t=\Lambda$) (m)
μ radial order of an acoustic duct mode
ρ_0 mean fluid density (kg m^{-3})
σ inter-blade phase angle ($\sigma=k_{x_{c0}}d+k_{y_{c0}}h=-2\pi m_g/B_I$)
ϕ acoustic potential (m^2 s^{-1})
$\Phi_{\mathrm{ww},i}$ PSD of the fluctuating upwash velocity divided by $w^2_{\mathrm{rms},i}$, i.e. PSD of $\overline{w}_i$ (m^3)
$\tilde{\Phi}_{\mathrm{ww},i}$ PSD of the fluctuating upwash velocity (m^5 s^{-2})
$\widehat{\Phi}_{ww}(k_{x_c},k_{z_c})$ two-dimensional spectrum of the non-dimensional upwash velocity (m^2)
$\check{\Phi}_{\mathrm{ww}}(\omega)$ PSD of the non-dimensional upwash velocity (s)
φ_I sweep angle after stagger and lean angle (rad)
$\check{\varphi}_I$ sweep angle in the duct reference frame (rad)
$\check{\chi}_I$ stagger angle in the duct reference frame of the cascade (rad)
$\chi=\arctan d/h$ rectilinear-cascade stagger angle (rad)
$\chi_{m,\mu}$ eigenvalue of the mode (m,μ) (m^{-1})
ψ_I stator lean angle after stagger angle (rad)
$\check{\psi}_I$ stator lean angle in the duct reference frame (rad)
$\Psi_{m,\mu}(\dot{r},\theta_d)e^{ik^{\pm}_{x_d,m\mu}x_d}$ duct eigenmodes ($\Psi_{m,\mu}(\dot{r},\theta_d)=E_{m,\mu}(\dot{r})e^{im\theta_d}$)
Ω_I cascade angular speed (rad s^{-1})
ω_{ex} incident angular frequency (rad s^{-1})
ω angular frequency (rad s^{-1})
$\omega_g=\omega_{\mathrm{ex}}-k_{z_{c0}}W$ modified angular frequency (rad s^{-1})

Subscripts

b relative to the ingested turbulence interacting with the rotor or to the background turbulence interacting with the stator
I $I\equiv R$ (relative to the rotor) or S (relative to the stator)
i $i\equiv b$ (relative to the background turbulence) or w (relative to the rotor-wake turbulence)
w relative to rotor-wake turbulence interacting with the stator

Superscripts

T matrix transpose
$*$ complex conjugate
$\pm$ refers to the radiation upstream and downstream of the blade row respectively

Abbreviations

LEE linearized Euler equations
PSD power spectral density
OGV outlet guide vanes
r.m.s. root mean square

1. Introduction

Turbofan engines with higher bypass ratios ensure improved aircraft performances at lower nominal rotation speed. Both the exhaust velocities of burnt gases and the corresponding jet noise are reduced and the fan-OGV (outlet guide vane) stage becomes a major contributor to the total noise. Modern very-high bypass architectures involve lower fan tip speed, reduced number of blades, selected blade and vane counts, and acoustic liners. This ensures tonal noise reduction and shifts the tone frequencies to lower values associated with weaker loudness. As a result, the broadband noise contribution is expected to become relatively more significant and dedicated prediction schemes are a crucial step to be included in the design cycles, as early and as accurately as possible. More specifically, the present study is dedicated to the prediction of the broadband noise resulting from the impingement of incident turbulence on a blade row either rotating or stationary. Numerical simulations of the turbulent compressible three-dimensional flow around the blades or the vanes could in principle reproduce all sound generation and propagation phenomena accurately, but are still a daunting task for an actual fan (blade span of the order of 1 m and Reynolds number based on the chord length and mean velocity around 10^6) and are far from being compatible with industrial time constraints. Besides, fan broadband noise prediction requires the whole power spectral density (PSD) of the acoustic power for frequencies ranging up to 10 kHz. Fast-running analytical models then appear to be still more appropriate in an industrial context.

Many studies have been performed over the past 40 years to predict the fan broadband noise caused by turbulence ingestion and wake interactions. Mugridge and Morfey [1], Mani [2], Hanson [3] and Sevik [4], among others, have dealt with the interaction of an incident turbulence with a rotating blade or a stationary vane. Homicz and George [5] extended these works to rotating blades at low frequencies and George and Kim [6] and Amiet [7] at high frequencies. Detailed reviews of the methods and experiments carried out during the seventies on rotor broadband noise were proposed by Cumpsty [8], Brooks and Schlinker [9] and George and Chou [10]. Most of these works were dedicated to open rotors, in particular the main rotor of a helicopter, for which the moderate blade number, often smaller than 10, allows using an isolated-airfoil response function.

Dealing with turbofan engines requires including the in-duct propagation in the prediction methods. Glegg [11], De Gouville [12] and Joseph and Parry [13] developed broadband noise models for ducted fans using Green's function tailored to the duct, and the unsteady blade loadings as acoustic sources. Glegg [11] dealt with the interaction of the rotor blades with the boundary layer of the casing and with the interaction of rotor wakes with the OGV. Yet the blades were assumed to be acoustically compact along the chord. De Gouville [12] resorted to Graham's similarity rules [14] to account for the compressibility effects and the non-compactness of the airfoil to determine the turbulence ingestion noise, while Joseph and Parry [13] used the two-dimensional compressible Amiet's function to predict the noise due to the interaction of the casing boundary layer with the rotor blades. These investigations were based on an isolated-airfoil response function. Nevertheless, current turbofan engines involve higher and higher bypass ratio and chord lengths, and the blade number of the rotor and the vane number of the stator can easily exceed 20 and 50 respectively (e.g. [15]). As a result, cascade effects must also be included in the prediction methods. Ventres et al. [16] were the first to propose a fan broadband noise model for inlet and wake turbulence considering both the duct and the cascade effects. These two aspects are an important theoretical improvement. An in-duct formulation of the acoustic analogy was applied, using the unsteady blade loading as input data, but resorting to a two-dimensional cascade response function. The radial variation of the turbulence was then taken into account by means of a strip theory. More recently Nallasamy and Envia [17] enhanced and coupled this model to a Reynolds-Averaged Navier–Stokes computation to get the turbulence input data for the acoustic model, showing a good agreement with measurements.

However, experimental results (e.g. [18]) show clear evidence of the strong spanwise variation of the turbulence in the rotor wakes developing upstream of the OGV, which may hinder the above two-dimensional decomposition of the impinging turbulence on stator vanes. Another approach then consists in including the spanwise variations of the turbulence by means of a three-dimensional rectilinear-cascade model: incident gusts are three-dimensional but the cascade is still considered rectilinear. Hanson [19] and Hanson and Horan [20] proposed a model for the interaction of a homogeneous or radially inhomogeneous incident turbulence with a rectilinear flat-plate cascade resorting to Glegg's cascade model [21]. Hanson then extended it to swept and leaned cascades [22] and to the broadband noise of a complete fan stage [23]. Glegg [24] and Glegg and Walker [25] accounted for the duct wall in the unwrapped configuration giving the exact solution to this approximate problem by means of a cosine functions basis. Evers and Peake [26] finally extended the method of Hanson and Horan [20] to include blade geometry effects. These predictions agreed quite well with the available experimental results despite the crucial assumption of rectilinear cascade [20]. Cheong et al. [27] again using a rectilinear-cascade model based on Smith's two-dimensional theory [28], pointed out a critical frequency, below which cascade effects are important, and only a part of the turbulent wavenumbers contribute to the resulting noise. Above that frequency, cascade effects can be neglected and the whole incident turbulence contributes. Jurdic et al. [29] predicted the rotor/stator interaction noise with this model using RANS data as inputs. Hanson's model and similar ones can be declined in a strip theory to take the radial variation of the geometry of an actual annular cascade into account. Yet, it directly applies to the radiated field and associated acoustic power, and does not rely on the unsteady blade loading as in the previous methods. As a result, the propagation in an annular duct cannot be accounted for.

Finally a significant improvement in fan broadband noise predictions has been recently achieved through three-dimensional unsteady linearized-Euler (LEE) simulations, fully accounting for the actual blade geometry. For instance,

Atassi and Vinogradov [30,31] and Atassi and Logue [32] proposed a very accurate fan broadband interaction noise method based on a previously developed model [33]. This approach noticeably accounts for the three-dimensional effects of the actual geometry, swirling mean flow and three-dimensional turbulence excitation and points out the importance of these parameters [33].

The present paper describes an analytical model of the broadband noise produced by turbulence in a rotor–stator arrangement. Both the interaction of ingested turbulence with the rotor blades and the rotor-wake impingement on downstream stator vanes are addressed. The model is a strip-theory application [34] based of a previously published formulation of the unsteady blade loading for a rectilinear cascade [35] and of the subsequent developments by the authors [34]. More precisely, Glegg's analytical formulation [21] has first been extended to provide closed-form expressions of the acoustic field valid inside the inter-blade channels, and of the unsteady-blade loading [35]. A wavenumber correction has also been proposed to include some of the three-dimensionality inherent to the annular configuration into the unwrapped description of a cascade strip in Cartesian coordinates [34]. This makes the unsteady blade loading calculated on each strip an equivalent dipole source distribution in an acoustic analogy formulation inside an annular duct. Preliminary broadband noise prediction issues have been addressed by Posson and Roger [36] and Posson et al. [37] to assess the effect of simplifying assumptions and the role of specific corrections to account for the main three-dimensional effects. The model was compared with the reference three-dimensional LEE computation of Atassi et al. [33] and with Logue and Atassi's updated version of the linear cascade model of Atassi and Hamad [38]. Posson and Roger [39] also carried out a dedicated experiment involving a turbulence grid upstream of a stationary cascade mounted at the exit section of an open-jet anechoic wind-tunnel. The model was found in a rather good agreement with the experiment in an extended low and middle frequency range. Further validations in configurations closer to a real engine were however recognized as necessary. The final version of the broadband noise model is described in detail in Section 2. The predictions are then compared, in Section 3, with the experimental data of the 22-in source diagnostic test (SDT) fan rig of the NASA Glenn Research Center [40–46]. Both numerical assessment and experimental validation are achieved.

2. Fan broadband noise model

Although three-dimensional features, such as swirl and non-uniform mean flow, induce significant aerodynamic effects (e.g. [47,48,33]), Atassi and Vinogradov showed that a simplified two-dimensional cascade model is adequate for predicting the fan broadband acoustic response at high frequencies [30,31]. Moreover, both Glegg's analytical formulation [24] and Hanson's model [20,22], based on a three-dimensional rectilinear-cascade response [21], were found successful in predicting the fan broadband noise caused by the interaction of an incident turbulence with an isolated blade row. For instance, Hanson and Horan [20] showed the ability of the model implemented in the code BFANS (e.g. Morin [49,50]) to be a design tool for rather realistic fans. Yet, some additional three-dimensional effects and further accuracy could be expected from coupling the cascade near-field information, such as the unsteady blade loading, with an acoustic analogy stated in an annular duct. This possible improvement motivated the present model developments that directly resort to the unsteady blade loading provided by the cascade response model. For a better geometrical representation, the annular duct is split into several strips. Each radial strip and its blade row part are unwrapped and assimilated to a rectilinear cascade having the local geometrical parameters embedded in a turbulent stream. The three-dimensional rectilinear-cascade response provides the unsteady blade loading distributed on the strip. This distribution is used as an equivalent dipole source in the acoustic analogy as an alternative to directly computing the radiated field. The turbulence is assumed to be locally homogeneous (assumption **H1**) and frozen (assumption **H2**) so that Taylor's hypothesis is introduced. The swirling mean flow effects on the sound propagation and on the distortion of the incident perturbations are ignored. The model can be considered as an extension of Ventres et al. [16] in the sense that it resorts to an acoustic analogy in an annular duct with uniform mean flow, as proposed by Goldstein [51] in circular duct, and to a cascade response function to compute the unsteady blade loading. Nevertheless, two important differences must be highlighted. Firstly, a three-dimensional response function is used in each strip instead of a two-dimensional one. Even if the radial variations of the geometry and of the mean flow features and turbulence are treated as parametric variations, the local three-dimensionality of the turbulence is introduced in the response function. Secondly, the formulation is written in cylindrical coordinates to reckon with the annular geometry and its effect on turbulence. Several developments in [16,17,22,51] are reproduced here in a unified way to stress the different assumptions used in the model and to emphasize the main differences and additions of the present work.

Until Sections 2.2 and 2.3 the developments apply indifferently to a rotor or a stator, the term blade will then be used indifferently for both a rotor blade and a stator vane. Section 2.2 will then focus on rotor blades and Section 2.3 on stator vanes. Several coordinate systems must be defined: $\mathcal{R}_d$ $(O_d,(x_d,y_d,z_d))$ a fixed reference frame attached to the duct with associated cylindrical coordinates (x_d,r_d,θ_d), $\mathcal{R}_l$ $(O_l,(x_l,y_l,z_l))$ a relative reference frame fixed to the annular blade row rotating at the speed Ω_l with associated cylindrical coordinates (x_l,r_l,θ_l), $\mathcal{R}_{cd}$ $(O_{cd},(x_{cd},y_{cd},z_{cd}))$ and $\mathcal{R}_c$ $(O_c,(x_c,y_c,z_c))$ two reference frames fixed to the rectilinear cascade at a particular radius r respectively before and after rotation of the sweep angle φ_l. The four coordinate systems are represented on a sketch of the annular duct with the blade row in Fig. 1(a), and the main geometrical parameters are defined in Fig. 1(b). The rotation matrices between the different reference frames, previously defined by Hanson [22], are reminded in Appendix A.1 with additional sketches in Fig. C1.

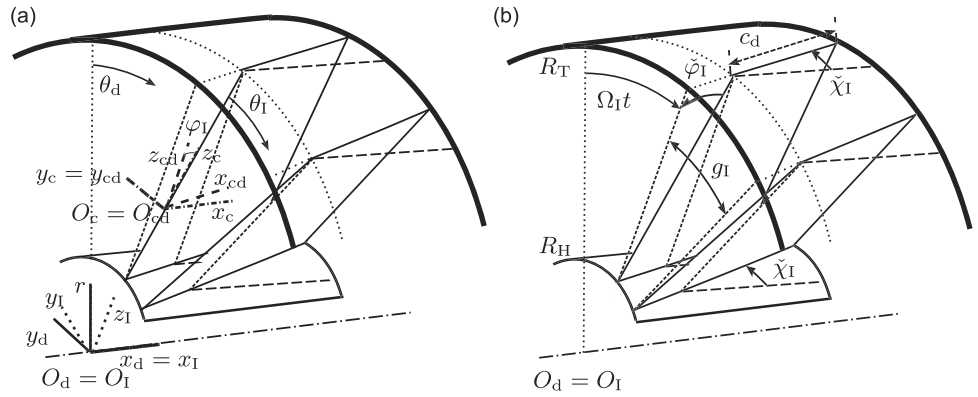

Fig. 1. Sketches of (a) the frames of reference used in the present model and (b) the geometrical parameters. Case of zero lean angle $\check{\psi}_I$.

To better account for the different scales of the problem and in particular those of turbulence, two non-dimensional variables are defined: the quickly varying coordinates $\check{\mathbf{x}} = \mathbf{x}/l_a$ which will be used to describe the local homogeneity and possible isotropy or axisymmetry of the turbulence around a radius, and the slowly varying coordinates $\hat{\mathbf{x}} = \mathbf{x}/R_T$, with in particular $\hat{r} = r/R_T$, which will be used to express the slow variation of turbulence characteristics and the geometry from one strip to a neighboring one. For instance, the cascade geometry, the turbulence intensity $\mathcal{T}_u$ and integral length scales ((l_a,l_t) or Λ), and the shape of the rotor wakes vary along the span but are assumed constant around a particular radius r inside a radial interval characterizing the fluctuations. Atassi and Vinogradov [30] dealt with the more general case where fluctuating velocities slowly vary in all directions due to swirling mean flow distortion effects.

2.1. Power spectral density of the acoustic power

Let us consider a fluid with mean density ρ_0, static pressure P_0, and temperature T_0 corresponding to a speed of sound c_0, moving at a mean velocity $\mathbf{U} = (U_{x_d},U_r,U_\theta)$ inside an annular duct of inner and outer radii R_H and R_T respectively. The sound produced by the impingement of turbulence on a blade row in the duct is characterized by the PSD of the acoustic power $S_{\mathrm{pp}}(\omega)$ at the angular frequency ω. The PSD can be expressed as a function of the acoustic pressure and velocity, as given for instance by Goldstein [51] for harmonic sources, or can be re-written as a function of the time-Fourier transform of the acoustic potential,

$$\Phi(\mathbf{x}_d,\omega) = \lim_{T\to\infty} \Phi_T(\mathbf{x}_d,\omega) \tag{1a}$$

with

$$\Phi_T(\mathbf{x}_d,\omega) = \frac{1}{2\pi}\int_{-T}^{T} \phi(\mathbf{x}_d,t)\, \mathrm{e}^{\mathrm{i}\omega t}\, \mathrm{d}t, \tag{1b}$$

in the form

$$S_{\mathrm{pp}}(\omega) = -\rho_0 \lim_{T\to\infty} \frac{\pi}{T} \mathrm{Re}\left(E\left[\int_S -\mathrm{i}\omega\Phi_T(\mathbf{x}_d,\omega)\left\{ \nabla\Phi(\mathbf{x}_d,\omega) - \frac{\mathbf{U}}{c_0^2}(\mathbf{U}\cdot\nabla\Phi_T(\mathbf{x}_d,\omega) - \mathrm{i}\omega\Phi_T(\mathbf{x}_d,\omega))\right\}^* \mathbf{n}\, \mathrm{d}\mathcal{S}\right]\right) \tag{2}$$

where $\mathbf{n}$ is the unit outward-normal vector of the elementary surface $\mathrm{d}\mathcal{S}$, $\mathbf{U}$ the mean velocity vector and the operator E denotes the expected value of the enclosed quantity. E is introduced since turbulence is treated as a random process. The radial component of the mean flow speed U_r is assumed to be zero (assumption **H3**). This hypothesis is very often valid in axial-flow turbomachines, since the fan design generally satisfies the radial equilibrium. The azimuthal component U_θ can also be neglected upstream of the fan rotor and downstream of the OGV, but its contribution is significant in-between. The azimuthal component must then be accounted for both in the distortion of the incident disturbance and in the sound propagation (e.g. [52–54,33]). In the present model, the properties of the incident turbulence are assumed to be known sufficiently close to the blade row of interest in order that their distortion by the mean flow can be neglected. Then the actual velocity triangle is used to convect the turbulent velocity field which is assumed frozen (assumption **H2**). The unsteady blade loading is calculated with the three-dimensional rectilinear-cascade model developed by Posson et al. [35,34]. The relative or total mean flow component U_0 is derived from the actual axial and azimuthal mean flow components, assuming zero angle of attack. The unsteady blade loading is then seen as an equivalent distribution of dipole sources in an acoustic analogy. In contrast, the acoustic field prediction assumes a uniform axial mean flow of Mach number $M_{x_d} = U_{x_d}/c_0$, which yields an analytical normal basis of eigenmodes. The acoustic potential can then be expanded on the eigenmodes of a rigid annular duct with uniform mean flow $\Psi_{m,\mu}(\hat{r},\theta_d)\mathrm{e}^{\mathrm{i}k^{\pm}_{x_d,m\mu}x_d} = E_{m,\mu}(\hat{r})\mathrm{e}^{\mathrm{i}k^{\pm}_{x_d,m\mu}x_d + \mathrm{i}m\theta_d}$, with

$$E_{m,\mu}(\hat{r}) = A_{m,\mu}J_m(\chi_{m,\mu}r) + B_{m,\mu}Y_m(\chi_{m,\mu}r). \tag{3}$$

The azimuthal and radial orders of the mode (m,μ) are the number of azimuthal nodes and the number of radial nodes respectively. The norm of the eigenmode is noted $\sqrt{\Gamma_{m,\mu}}$ and the eigenvalue of $E_{m,\mu}$ is $\chi_{m,\mu}$. The acoustic potentials in the upstream (+) and downstream (−) directions are then expressed as

$$\Phi^{\pm}(\mathbf{x}_d,\omega)=\sum_{m\in\mathbb{Z}}\sum_{\mu\in\mathbb{N}}\Phi^{\pm}_{m,\mu}(\omega)\,E_{m,\mu}(\dot{r})\,\mathrm{e}^{\mathrm{i}k^{\pm}_{x_d,m\mu}x_d+\mathrm{i}m\theta_d}, \tag{4a}$$

with the modal amplitudes

$$\Phi^{\pm}_{m,\mu}(\omega)=\frac{\mathcal{P}^{\pm}_{m,\mu}(\omega)}{\mathrm{i}\rho_0[\omega-k^{\pm}_{x_d,m\mu}\underline{U_{x_d}}]}, \tag{4b}$$

where $\mathcal{P}^{\pm}_{m,\mu}(\omega)$ is the pressure amplitude of the duct mode (m,μ). The acoustic powers $S^{\pm}_{\mathrm{pp}}$ are obtained by replacing Φ by its expressions (4a) and $\mathcal{S}$ by two duct sections upstream and downstream of the blade row, of unit outward-normal vector $\mathbf{n}^{\pm}=\mp(1,0,0)$ respectively, in Eq. (2). The acoustic PSD is finally written as the sum of the acoustic powers of all cut-on duct modes:

$$S^{\pm}_{\mathrm{pp}}(\omega)=\sum_{m\in\mathbb{Z}}\sum_{\mu\in\mathbb{N}}\mathrm{Re}\left(F^{\pm}_{m,\mu}\lim_{T\to\infty}\frac{\pi}{T}E[|\mathcal{P}^{\pm}_{m,\mu}(\omega)|^2]\right), \tag{5a}$$

$\lim_{T\to\infty}(\pi/T)\,E[|\mathcal{P}^{\pm}_{m,\mu}(\omega)|^2]$ is the expected value of the power density of the duct mode (m,μ) and

$$F^{\pm}_{m,\mu}=\frac{\Gamma_{m,\mu}}{\rho_0 c_0}\,G^{\pm}_{m,\mu},\quad G^{\pm}_{m,\mu}=\frac{\kappa^{*}_{m,\mu}k_0}{|k_0-k^{\pm}_{x_d,m\mu}M_{x_d}|^2},\quad k_0=\frac{\omega}{c_0},$$

$$\kappa^2_{m,\mu}=k_0^2-\beta^2_{x_d}\chi^2_{m,\mu},\quad k^{\pm}_{x_d,m\mu}=\frac{-k_0M_{x_d}\mp\kappa_{m,\mu}}{\beta^2_{x_d}},\quad \beta_{xd}=\sqrt{1-M^2_{x_d}}, \tag{5b}$$

where the superscript $*$ stands for the complex conjugate.

The acoustic analogy in an annular duct with uniform mean flow provides an expression for the noise due to the interaction of a row of B_I blades or vanes (I stands either for the rotor $I=R$ or the stator $I=S$) with an incident gust, as given by Posson et al. [34] and, by extension, with an incident turbulence as detailed by Ventres et al. [16]. The problem only involves time-stationary processes. The acoustic pressure $p^{\pm}(\mathbf{x}_d,t)$ at point $\mathbf{x}_d$ and time t is determined by the unsteady force per unit area $\mathbf{f}(\mathbf{x}_{d0},t_0)$ on the blade/vane surfaces $(\bigcup_{j\in[0,B_I-1]}S^t_j(t_0))$ and Green's function tailored to the annular duct in uniform axial mean flow $G_d(\mathbf{x}_d,t|\mathbf{x}_{d0},t_0)$ [51]:

$$p^{\pm}(\mathbf{x}_d,t)=\int_{-T}^{T}\iint_{\bigcup_j S^t_j(t_0)}\frac{\partial G_d(\mathbf{x}_d,t|\mathbf{x}_{d0},t_0)}{\partial n}\,\mathbf{f}(\mathbf{x}_{d0},t_0)\,\mathrm{d}S(\mathbf{x}_{d0})\,\mathrm{d}t_0. \tag{6}$$

Only the dipole-like sources are considered in Eq. (6); monopoles and quadrupoles are ignored. Since the viscous forces are neglected, the net force on a surface reduces to the pressure force $\mathbf{f}=p\mathbf{n}$ where $\mathbf{n}$ is the surface outward-normal unit vector and p the pressure on the surface. Moreover the blades are assumed to be flat plates, and the normal vectors $\mathbf{n}^s_j$ and $\mathbf{n}^p_j$, on the suction and pressure sides of the blade j respectively, are opposite: $\mathbf{n}^s_j=-\mathbf{n}^p_j=\mathbf{n}_j$. The elementary force $\mathbf{f}(\mathbf{x}_{d0},t_0)\,\mathrm{d}S_j$ across the blade j on the elementary surface $\mathrm{d}S_j$ reduces to

$$\mathbf{f}(\mathbf{x}_{d0},t_0)\,\mathrm{d}S_j=[p^s(\mathbf{x}_{d0},t_0)-p^p(\mathbf{x}_{d0},t_0)]\,\mathrm{d}S_j\,\mathbf{n}_j=-\Delta P(\mathbf{x}_{d0},t_0)\,\mathrm{d}S_j\,\mathbf{n}_j, \tag{7}$$

where ΔP is the pressure jump. S_j is the surface of the blade j which spins at angular frequency Ω_I. A change from the reference frame $\mathcal{R}_d$ to the reference frame rotating with the blades $\mathcal{R}_I$ is introduced to evaluate the unsteady loading on a blade. By definition, the azimuthal coordinates are related by $\theta_{d0}=\theta_{I0}+\Omega_I t_0$. In the frame of reference $\mathcal{R}_I$, the surface $S_{j,I}$ of the blade j is stationary. The integrals in Eq. (6) can then be inverted, and the following property is used:

$$\lim_{T\to\infty}\int_{-T}^{T}\mathrm{e}^{\mathrm{i}(\omega-m\Omega_I)t_0}\Delta P(\mathbf{x}_{I0},t_0)\,\mathrm{d}t_0=2\pi\Delta\widehat{P}(\mathbf{x}_{I0},\omega-m\Omega_I), \tag{8}$$

where $\Delta\widehat{P}(\mathbf{x}_{I0},\omega_{ex})$ is the Fourier transform of $\Delta P(\mathbf{x}_{I0},t_0)$ in time. The pressure can be Fourier transformed and expanded on the duct modes. The expression of the complex amplitude of the pressure of the duct mode (m,μ) is then equal to

$$\mathcal{P}^{\pm}_{m,\mu}(\omega)=\int_{\bigcup_j S_{j,I}}\frac{\Delta\widehat{P}(\mathbf{x}_{I0},\omega-m\Omega_I)}{2i\kappa_{m,\mu}\Gamma_{m,\mu}}\,\mathbf{n}_{j,I}\cdot\nabla_{\mathbf{n}_{j,I}}[E^{*}_{m,\mu}(r_0)\mathrm{e}^{-\mathrm{i}m\theta_{I0}-\mathrm{i}k^{\pm}_{x_I,m\mu}x_{I0}}]\,\mathrm{d}S_j(\mathbf{x}_{I0}). \tag{9}$$

The contribution of the duct mode of azimuthal order m to the pressure at frequency ω is produced by the interaction of the cascade with the gust at frequency $\omega_m=\omega-m\Omega_I$. The rotating blade row thus induces a frequency scattering in addition to the modal scattering. Since all blades are identical, evenly spaced and labelled by ascending numbers along y_I, like in Fig. 2, the coordinates of point M_j of the blade j corresponding to point $M_0(x_{I0},r_0,\theta_{I0})$ of the blade 0 are $M_j(x_{I0},r_0,\theta_{I0}-2\pi j/B)$. The unit vector $\mathbf{n}_{0,I}$ normal to the blade 0, defined as $\mathbf{u}_{y,cd}=\mathbf{u}_{y,c}$ in the cascade reference frame R_{cd},

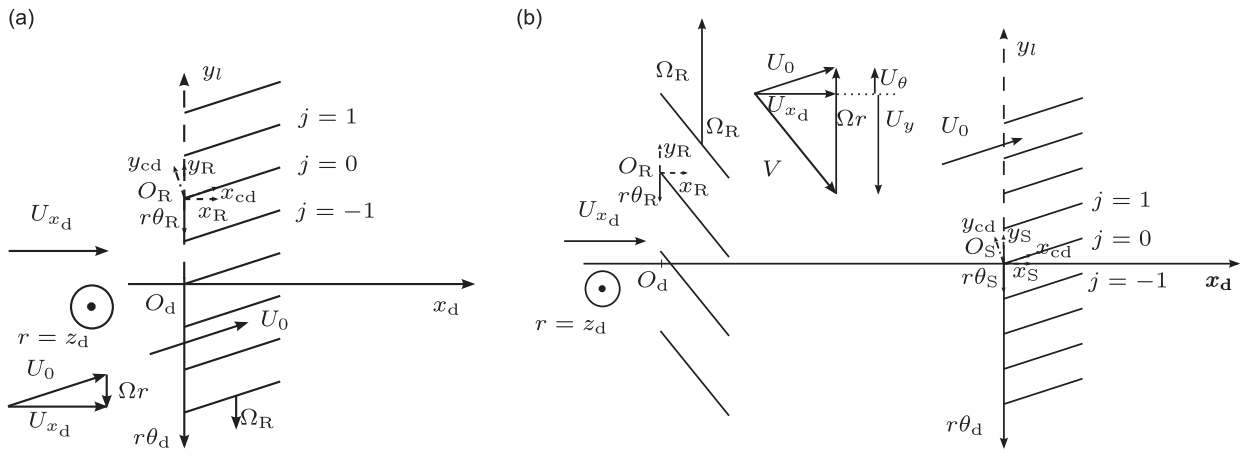

Fig. 2. Sketch of the rotor and the stator in an unwrapped view at radius r, including the mean velocity triangles and the coordinate systems: (a) incident turbulence impinging on a rotor; (b) rotor wakes and background turbulence impinging on a stator.

and the gradient vector $\nabla_{\mathbf{n}_{0,I}}$ are defined in the duct reference frame $\mathcal{R}_I$ in Cartesian coordinates to yield

$$\mathbf{n}_{0,I}=(\mathbf{u}_{y,cd})_I=(\mathbf{u}_{y,c})_I=\mathbf{Q}_{\mathrm{inv},I}\bullet\mathbf{u}_{y,c}=\mathbf{Q}_{\check{\chi}\psi\phi,I}(2,:)=\mathbf{q}_I,$$

$$\nabla_{\mathbf{n}_{0,I}}=\left(\frac{\partial}{\partial r_0},\frac{\partial}{r_0\partial\theta_{I0}},\frac{\partial}{\partial x_{I0}}\right). \tag{10}$$

These developments generalize those of Ventres et al. [16] to any blade row. The sweep $\check{\varphi}_I$ and lean $\check{\psi}_I$ angles can now be non-zero and vary radially. The definitions of the geometry and of the successive changes of reference frames match Hanson's developments and conventions [22]. The transformation matrices $\mathbf{Q}_{\check{\chi}\psi\phi,I}$ and $\mathbf{Q}_{\mathrm{inv},I}$ are detailed in Appendix A.1. The complex amplitude of the duct mode (m,μ) finally reads

$$\mathcal{P}^{\pm}_{m,\mu}(\omega)=\frac{1}{2\kappa_{m\mu}\Gamma_{m\mu}}\int_{R_H}^{R_T}S^{\pm}_{m\mu}(\grave{r},\omega)\int_0^{c_d(\grave{r})}\sum_{j=0}^{B_I-1}\mathrm{e}^{\mathrm{i}j2\pi m/B_I}\Delta\widehat{P}_{cd,j}(x_{cd},\grave{r},\omega_m)\mathrm{e}^{-\mathrm{i}k^{\pm}_{x_{cd},m\mu}(\grave{r})x_{cd}}\mathrm{e}^{\mathrm{i}(m/r)y_{\mathrm{LE},I}(\grave{r})-\mathrm{i}k^{\pm}_{x_I,m\mu}x_{\mathrm{LE},I}(\grave{r})}\,\mathrm{d}x_{cd}\,\mathrm{d}r, \tag{11a}$$

where

$$S^{\pm}_{m\mu}(\grave{r},\omega)=\zeta^{\pm}_{m,\mu}(\grave{r})E_{m,\mu}(\grave{r}),\quad \zeta^{\pm}_{m,\mu}(\grave{r})=\left[-\mathrm{i}q_{3,I}\frac{\mathrm{d}E_{m,\mu}(\grave{r})}{E_{m,\mu}(\grave{r})\mathrm{d}r}+\left(q_{2,I}\frac{m}{r}-q_{1,I}k^{\pm}_{x_I,m\mu}\right)\right], \tag{11b}$$

$x_{\mathrm{LE},I}$ and $y_{\mathrm{LE},I}$ are leading-edge distances defined in Eq. (A.4) of Appendix A.1, and $k^{\pm}_{x_{cd},m\mu}(\grave{r})=Q_{\check{\chi}\psi,I,11}k^{\pm}_{x_d,m\mu}-Q_{\check{\chi}\psi,I,12}m/r$ is the axial wavenumber of the duct mode (m,μ) in the cascade frame of reference $\mathcal{R}_{cd}$ before the rotation of sweep angle [22]. $\Delta\widehat{P}_{cd,j}(x_{cd},\grave{r},\omega_{\mathrm{ex}})$ is the pressure jump at the radius r, on the blade j, for a chordwise position x_{cd} in the cascade frame of reference $\mathcal{R}_{cd}$ at the angular frequency of the incident excitation ω_{ex}. Unlike the harmonic gust, considered by Posson et al. [34] in the Third Computational Aeroacoustic benchmark [55], the unsteady flow excitation is here a turbulent flow. The only random parameter in Eq. (11a) is actually the unsteady blade loading, leading to the term $S^{(j,j')}_{\mathrm{FF},cd}(x_{cd},r,\omega;x'_{cd},r',\omega)$ in the expected value of the spectrum of the duct modes in Eq. (12a).The latter is the cross-spectrum of the unsteady blade loadings at point M (x_{cd},r) on blade j and at point M′ (x'_{cd},r') on blade j' at angular frequencies ω and ω' defined in Eq. (12b).

A radial length L_r is now assumed to exist beyond which the cross-correlation of the unsteady blade loading goes to zero (**H4**). The cascade geometry and the flow properties are also considered unchanged over an extent $l_r=2L_r$. This is the second part of assumption **H4**. The radial correlation length l_r is taken in practice as the radial correlation length of the incident, locally isotropic or axisymmetric homogeneous turbulence. Under this assumption, the expected value of the spectrum of the duct mode (m,μ) is written as

$$\begin{aligned}\lim_{T\to\infty}\frac{\pi}{T}E[|\mathcal{P}_{m,\mu}(\omega)|^2]=\left(\frac{1}{2|\kappa_{m\mu}|\Gamma_{m\mu}}\right)^2\int_{R_H}^{R_T}\int_{r-L_r}^{r+L_r}S^{\pm}_{m,\mu}(\grave{r},\omega)S^{\pm}_{m,\mu}(\grave{r}',\omega)^*\int_0^{c_d(\grave{r})}\int_0^{c_d(\grave{r}')}\mathrm{e}^{-\mathrm{i}(k^{\pm}_{x_{cd},m\mu}(\grave{r})x_{cd}-k^{\pm}_{x_{cd},m\mu}(\grave{r}')x'_{cd})}\\ \times\sum_{j=0}^{B_I-1}\sum_{j'=0}^{B_I-1}\mathrm{e}^{\mathrm{i}(j-j')2\pi m/B_I}S^{(j,j')}_{\mathrm{FF},cd}(x_{cd},r,\omega_m;x'_{cd},r',\omega_m)\,\mathrm{d}x_{cd}\,\mathrm{d}x'_{cd}\\ \times\mathrm{e}^{-\mathrm{i}(m/r')y_{\mathrm{LE},I}(\grave{r}')+\mathrm{i}k^{\pm}_{x'_I,m\mu}x_{\mathrm{LE},I}(\grave{r}')}\mathrm{d}r'\mathrm{e}^{\mathrm{i}(m/r)y_{\mathrm{LE},I}(\grave{r})-\mathrm{i}k^{\pm}_{x'_I,m\mu}x_{\mathrm{LE},I}(\grave{r})}\,\mathrm{d}r,\end{aligned} \tag{12a}$$

where

$$S^{(j,j')}_{\mathrm{FF},cd}(x_{cd},r,\omega_m;x'_{cd},r',\omega'_m)=\lim_{T\to\infty}\frac{\pi}{T}E[\Delta\widehat{P}_{cd,j}(x_{cd},r,\omega_m)\Delta\widehat{P}_{cd,j}(x'_{cd},r',\omega'_m)^*]. \tag{12b}$$

The distribution of the unsteady loading must be computed at all points on the blade. From the formulation (12a), it is useful to scan each radius r and then to scan every chordwise position at constant radius, that is to say to scan x_{cd} in the cascade frame of reference before sweep $\mathcal{R}_{cd}$ as proposed by Posson [34]. Assumption **H4** and the following developments related to l_r lead to an important difference with the approach of Ventres et al. [16] or Nallasamy and Envia [17], who assume that the radial integral length scale is very small compared to the duct radius. Consequently, in their approach the difference of radii is neglected in all terms except in the radial correlation function.

Two different noise mechanisms are now investigated. The interaction of an incident turbulence with a rotor, sketched in Fig. 2(a) is first presented in Section 2.2 . The interaction of turbulent rotor wakes and background turbulence with a stator, sketched in Fig. 2(b) is then discussed in Section 2.3.

2.2. Interaction of ingested turbulence with the rotor

2.2.1. Statistical properties of the turbulence

Since the incident disturbance on the rotor corresponds to ingested turbulence, its properties are considered in the stationary frame of reference $\mathcal{R}_d$. From Taylor's hypothesis **H2**, the turbulence is simply convected by the mean flow, so that the upwash velocity is written as

$$\mathbf{u}(\mathbf{x}_d,t)\cdot\mathbf{n}_c = w_b(\mathbf{x}_d,t) = \check{w}_b(\mathbf{x}_d - tU_{x_d}(\grave{r})\mathbf{e}_{x_d}), \tag{13}$$

where $\check{w}_b(\mathbf{x}_d)$ is the upwash component of the incident gust in the frame of reference $\mathcal{R}_f$ attached to the axial mean flow upstream of the rotor. The assumption of locally homogeneous turbulence allows writing

$$\check{w}_b(\mathbf{x}_d) = w_{\mathrm{rms,b}}(\grave{r})\overline{w}_b(\check{\mathbf{x}}_d\,|\,\grave{r}), \tag{14}$$

where $\overline{w}_b$ is a stochastic variable in the interval $[-1,1]$. The amplitude $w_{\mathrm{rms,b}}$ and the integral length scales (l_a,l_t) or Λ involved in $\overline{w}_b$ only depend on the slowly varying coordinate $\check{r}$. The turbulence itself is nearly isotropic or axisymmetric in the vicinity of the radius r. A Liepmann or an axisymmetric-turbulence model is then assumed to describe the spectrum of the non-dimensional velocity $\overline{w}_b(\check{\mathbf{x}}_d,\grave{r})$. The former only depends on the turbulence intensity $w_{\mathrm{rms},i}$ and the integral length scale Λ_i (see Appendix C.1). In the chosen formulation detailed in Section 2.5 and Appendix C.2, the latter is expressed as a function of the turbulence intensity $w_{\mathrm{rms},i}$ and the longitudinal and transverse integral length scales $(l_{a,i},l_{t,i})$. Besides, $\check{w}_b$ and w_b are periodic functions of the azimuthal angle because the turbulence is analyzed in a duct. Since the turbulence interacts with the rotor, the cross-spectrum of the upwash velocity must be given in the cascade frame of reference of the rotor $\mathcal{R}_c$ (or $\mathcal{R}_{cd}$) in which the unsteady blade loading is expressed. To do so, the intermediate frame of reference $\mathcal{R}_R$ must be introduced. In this reference frame, the Fourier transform yields

$$\check{w}_{m_g}(k_{x_R},k_{z_{R0}},\omega) = \frac{1}{(2\pi)^4}\iiint_{\mathbb{R}^3}\int_{-\pi}^{\pi} w_b(\mathbf{x}_d,t)\mathrm{e}^{\mathrm{i}\omega t+\mathrm{i}k_{x_R}x_R-\mathrm{i}m_g\theta_R-\mathrm{i}k_{z_{R0}}r}\,\mathrm{d}\theta_d\,\mathrm{d}r\,\mathrm{d}x_R\,\mathrm{d}\omega. \tag{15}$$

The variables being stochastic, the expected value of the turbulent inflow wavenumber frequency spectrum, S_{WW}, must be introduced. It is defined as

$$S_{\mathrm{WW}} = \sum_{m_g\in\mathbb{Z}}\sum_{m'_g\in\mathbb{Z}} S_{\mathrm{WW}}^{m_g,m'_g} \tag{16a}$$

with

$$\begin{aligned} S_{\mathrm{WW}}^{m_g,m'_g} &= \langle w_{m_g}(k_{x_R},k_{z_{R0}},\omega)w'_{m_g}(k'_{x_R},k'_{z_{R0}},\omega')^*\rangle \\ &= \frac{1}{(2\pi)^2}\iint_{\mathbb{R}^2}\frac{1}{(2\pi)^2}\iint_{[-\pi,\pi]^2}\frac{1}{(2\pi)^2}\iint_{\mathbb{R}^2}\frac{1}{(2\pi)^2}\iint_{\mathbb{R}^2}\langle w_b(\mathbf{x}_d,t)w_b(\mathbf{x}'_d,t')^*\rangle \\ &\times\mathrm{e}^{\mathrm{i}\omega t-\mathrm{i}\omega' t'}\,\mathrm{d}t\,\mathrm{d}t'\,\mathrm{e}^{\mathrm{i}k_{x_R}x_R-\mathrm{i}k_{x'_R}x'_R}\,\mathrm{d}x_R\,\mathrm{d}x'_R\times\mathrm{e}^{-\mathrm{i}(m_g\theta_R-m'_g\theta'_R)}\,\mathrm{d}\theta_R\,\mathrm{d}\theta'_R\,\mathrm{e}^{-\mathrm{i}(k_{z_{R0}}r-k_{z'_{R0}}r')}\mathrm{d}r\,\mathrm{d}r'. \end{aligned} \tag{16b}$$

Introduce now the quantities:

$$\Upsilon = k_{x_R}x_R - m_g\theta_R - k_{z_{R0}}r, \quad \Upsilon^\star = k'_{x_R}x'_R - m'_g\theta'_R - k_{z_{R0}}r', \tag{17a}$$

and the distance $\boldsymbol{\xi}$ between the two points $\mathbf{x}_d - tU_{x_d}(\grave{r})\mathbf{e}_{x_d}$ and $\mathbf{x}'_d - t'U_{x_d}(\grave{r}')\mathbf{e}_{x_d}$. In the absolute frame of reference $\mathcal{R}_d$ $\boldsymbol{\xi}$, reads

$$\boldsymbol{\xi} = \mathbf{x}_{\mathrm{d}'} - U_{x_d}(\grave{r}')\mathbf{e}_{x_d}t' - \mathbf{x}_d + U_{x_d}(\grave{r})\mathbf{e}_{x_d}t = (r'-r,\theta'_d-\theta_d,x'_d-x_d-U_{x_d}(\grave{r}')t'+U_{x_d}(\grave{r})t) = (\xi_r,\xi_\theta,\xi_x). \tag{17b}$$

The phase term in the complex exponential of Eq. (16b) follows as

$$\begin{aligned} \Upsilon-\Upsilon^\star+\omega t-\omega' t' = {} & [k_{x_R}-k'_{x_R}]x_d-(m_g-m'_g)\theta_d-(k_{z_{R0}}-k'_{z_{R0}})r-k'_{x_R}\xi_x+m'_g\xi_\theta+k'_{z_{R0}}\xi_r+[\omega+k'_{x_R}U_{x_d}(\grave{r})+m_g\Omega_R]t \\ & -[\omega'+k'_{x_R}U_{x_d}(\grave{r}')+m'_g\Omega_R]t'. \end{aligned} \tag{18}$$

Further neglecting the differences between the mean velocities U_{x_d} and the turbulence intensities $w_{\mathrm{rms},b}$ at radii $\grave{r}$ and $\grave{r}'$, which is valid whenever $|r-r'|\le l_r$ from assumption **H4**, Eq. (16b) becomes

$$S_{\mathrm{WW}}^{m_g,m_g'} = \frac{1}{(2\pi)^6}\iint_{\mathbb{R}^2}\iint_{[-\pi,\pi]^2}\iint_{\mathbb{R}^2} \mathrm{e}^{\mathrm{i}[k_{x_R}-k'_{x_R}]x_d}\,\mathrm{e}^{-\mathrm{i}(m_g-m_g')\theta_d}\,\mathrm{e}^{-\mathrm{i}(k_{z_{\mathrm{R}0}}-k'_{z_{\mathrm{R}0}})r} \times\delta(\omega+k'_{x_R}U_{x_d}(\dot{r})+m_g\Omega_R)\delta(\omega'-\omega+(m_g'-m_g)\Omega_R) \times w_{\mathrm{rms,b}}(\dot{r})^2\langle\overline{w}_b(\check{\mathbf{x}}_d-tU_{x_d}(\dot{r})\mathbf{e}_{x_d},\dot{r})\overline{w}_b(\check{\mathbf{x}}'_d-t'U_{x_d}(\dot{r})\mathbf{e}_{x_d},\dot{r})^*\rangle \times\mathrm{e}^{-\mathrm{i}k'_{x_R}\xi_x+\mathrm{i}m'_g\xi_\theta+\mathrm{i}k'_{z_{\mathrm{R}0}}\xi_r}\,\mathrm{d}x_R\,\mathrm{d}\xi_x\,\mathrm{d}\theta_d\,\mathrm{d}\xi_\theta\,\mathrm{d}r\,\mathrm{d}\xi_r. \tag{19}$$

In addition, the assumption of local homogeneous turbulence (**H1**) yields

$$\langle\overline{w}_b(\check{\mathbf{x}}_d-tU_{x_d}(\dot{r})\mathbf{e}_{x_d},\dot{r})\overline{w}_b(\check{\mathbf{x}}'_d-t'U_{x_d}(\dot{r})\mathbf{e}_{x_d},\dot{r})^*\rangle = \mathcal{R}_{nn,\mathrm{b}}(\boldsymbol{\xi},\dot{r}), \tag{20}$$

where $\mathcal{R}_{nn,\mathrm{b}}$ is the cross-correlation function of the upwash velocity which slowly varies with the radius seen as a mere parameter. By definition:

$$\mathcal{R}_{nn,\mathrm{b}}(\Delta\boldsymbol{x},\dot{r}) = \iiint_{\mathbb{R}^3}\Phi_{\mathrm{ww,b}}(\mathbf{K}''_R,\dot{r})\mathrm{e}^{\mathrm{i}\mathbf{K}''_R\cdot\Delta\boldsymbol{x}}\,\mathrm{d}\mathbf{K}''_R, \tag{21}$$

where $\Phi_{\mathrm{ww,b}}$ is the PSD of the fluctuating upwash velocity divided by $w_{\mathrm{rms,b}}(\dot{r})^2$, i.e. the PSD of $\overline{w}_b$. Then the integrations over x_R, θ_d, and r are equal to the product of two Dirac delta functions and a Kronecker term: $\delta(k_{x_R}-k'_{x_R})$, $\delta(k'_{z_{\mathrm{R}0}}-k_{z_{\mathrm{R}0}})$ and δ'_{m_g,m_g}. The triple integrals over the vector $\boldsymbol{\xi}$ must be calculated in Cartesian coordinates to be consistent with the three-dimensional spectrum Φ_{ww}. The difference between the radii is neglected in the coordinates $y_{\mathrm{l}}=-r\theta_d$ and y'_{l}, thus $y_{\mathrm{l}}-y'_{\mathrm{l}}\approx-r\xi_\theta$. The integrations then read

$$\int_{\mathbb{R}^2}\int_{-\pi}^{\pi}\frac{\mathcal{R}_{nn,\mathrm{b}}(\xi,\dot{r})}{(2\pi)^3}\mathrm{e}^{-\mathrm{i}k'_{x_R}\xi_x+\mathrm{i}m'_g\xi_\theta+\mathrm{i}k'_{z_{\mathrm{R}0}}\xi_r}\,\mathrm{d}\xi_\theta\,\mathrm{d}\xi_x\,\mathrm{d}\xi_r = \frac{1}{r}\Phi_{\mathrm{ww,b}}\left(-k'_{x_R},-\frac{m_g}{r},k'_{z_{\mathrm{R}0}},\dot{r}\right). \tag{22}$$

Finally, the upwash expected value of the ingested turbulence associated with modes m_g, m'_g, $S_{\mathrm{WW}}^{m_g,m'_g}$, is written as

$$S_{\mathrm{WW}}^{m_g,m'_g} = \frac{w_{\mathrm{rms,b}}(\dot{r})^2}{r}\delta(\omega+m_g\Omega_R-k_{x_{\mathrm{R}0}}U_{x_d}(\dot{r}))\delta(\omega'-\omega)\Phi_{\mathrm{ww,b}}(\mathbf{K}_{\mathrm{R}0},\dot{r})\delta(k'_{x_{\mathrm{R}0}}-k_{x_{\mathrm{R}0}})\delta'_{m_g,m_g}\delta(k'_{z_{\mathrm{R}0}}-k_{z_{\mathrm{R}0}}), \tag{23}$$

where

$$\mathbf{K}_{\mathrm{R}0} = \left(k_{x_{\mathrm{R}0}},-\frac{m_g}{r},k_{z_{\mathrm{R}0}}\right)$$

with $k_{x_{\mathrm{R}0}}=-k_{x_R}$. This result also supposes that Λ is small compared with the radial variation of the excitation, i.e. that the two radii can be taken equal in the amplitude terms. The three-dimensional spectrum of the upwash velocity of the locally homogeneous turbulence Φ_{ww} will be modelled in Section 2.5.

2.2.2. Expected value of the unsteady blade loadings

The incident turbulent flow must be expressed in the rotor frame of reference $\mathcal{R}_R$ and finally in the local cascade frame of reference $\mathcal{R}_c$ for the sake of applying the cascade response function. Using the Fourier coefficients $\check{w}_{m_g}(k_{x_R},k_{z_{\mathrm{R}0}},\omega)$ introduced in the previous section, the fluctuating upwash velocity is expanded as

$$w_b(\mathbf{x}_R,t) = \int\sum_{m_g\in\mathbb{Z}}\iint\check{w}_{m_g}(k_{x_R},k_{z_{\mathrm{R}0}},\omega)\mathrm{e}^{\mathrm{i}k_{z_{\mathrm{R}0}}r}\mathrm{e}^{-\mathrm{i}\mathbf{K}_R\cdot\mathbf{x}_R-\mathrm{i}\omega t}\,\mathrm{d}k_{z_{\mathrm{R}0}}\,\mathrm{d}k_{x_R}\,\mathrm{d}\omega, \tag{24}$$

where $\exp(\mathrm{i}k_{z_{\mathrm{R}0}}r)$ stands for the phase shift due to the radial position in the three-dimensional blade row. The wavenumber vector in the cascade frame of reference $\mathbf{K}_c$ is related to the wavenumber vector in the rotor frame of reference $\mathbf{K}_R$ by $\mathbf{K}_c=\mathbf{Q}\cdot\mathbf{K}_R=\mathbf{Q}\cdot(k_{x_R},m_g/r,-k_{z_{\mathrm{R}0}})^T$. The incident wavenumber vector is $\mathbf{K}_{c0}=(k_{x_{c0}},k_{y_{c0}},k_{z_{c0}})=-\mathbf{K}_c$ and the associated inter-blade phase angle is $\sigma=-2\pi m_g/B_R$. Then, the incident disturbance on the blade in the cascade frame of reference is expanded as

$$w_b(\mathbf{x}_c,t) = -\int\sum_{m_g\in\mathbb{Z}}\iint\check{w}_{m_g}(-k_{x_{\mathrm{R}0}},k_{z_{\mathrm{R}0}},\omega)\mathrm{e}^{\mathrm{i}k_{z_{\mathrm{R}0}}r}\mathrm{e}^{\mathrm{i}\mathbf{K}_{c_0}\cdot\mathbf{x}_c-\mathrm{i}\omega t}\,\mathrm{d}k_{z_{\mathrm{R}0}}\,\mathrm{d}k_{x_{\mathrm{R}0}}\,\mathrm{d}\omega. \tag{25}$$

The associated unsteady response on the reference blade 0 at radius r is expressed as

$$\Delta p_c(x_c,z_c,t) = -\rho_0(\dot{r})c_0(\dot{r})\int\sum_{m_g\in\mathbb{Z}}\iint\check{w}_{m_g}(-k_{x_{\mathrm{R}0}},k_{z_{\mathrm{R}0}},\omega)\mathrm{e}^{\mathrm{i}k_{z_{\mathrm{R}0}}r}\Delta\widehat{P}_{c,0}(x_c,\omega|\dot{r})\mathrm{e}^{\mathrm{i}k_{z_{c0}}z_c-\mathrm{i}\omega t}\,\mathrm{d}k_{z_{\mathrm{R}0}}\,\mathrm{d}k_{x_{\mathrm{R}0}}\,\mathrm{d}\omega, \tag{26}$$

where $\Delta\widehat{P}_{c,0}(x_c,\omega|\dot{r})$ is the pressure jump made non-dimensional by $\rho_0c_0w_0$ produced by a gust of amplitude w_0, inter-blade phase angle σ, radial wavenumber $k_{z_{c0}}$ and angular frequency ω, on the rectilinear cascade having the local geometry of the blade row. From Eq. (12a), the Fourier transform of the unsteady blade loading $\Delta p_c(x_{cd},r,t)$, $\Delta\widehat{P}_{cd,j}(x_{cd},\dot{r},\omega)$, must be computed for each radius at every chordwise position at constant radius, x_{cd}, in the cascade frame of reference before sweep $\mathcal{R}_{cd}$. Posson et al. [34] showed that

$$\Delta\widehat{P}_{cd,j}(x_{cd},\dot{r},\omega)\approx\Delta\widehat{P}_{c,j}(x_{cd}\cos\varphi,\omega|\dot{r})\mathrm{e}^{\mathrm{i}k_{z_{c0}}\sin\varphi x_{cd}}, \tag{27a}$$

with

$$\Delta\widehat{P}_{c,j}(x_c,\omega|\grave{r}) = \Delta\widehat{P}_{c,0}(x_c,\omega|\grave{r})\mathrm{e}^{\mathrm{i}j\sigma}. \tag{27b}$$

As a result, the Fourier transform reads

$$\Delta\widehat{P}_{cd,j}(x_{cd},r,\omega) = -\rho_0 c_0 \sum_{m_g\in\mathbb{Z}} \iint \check{w}_{m_g}(-k_{x_{\mathrm{R}0}},k_{z_{\mathrm{R}0}},\omega)\mathrm{e}^{\mathrm{i}k_{z_{\mathrm{R}0}}r}\Delta\widehat{P}_{c,0}(x_{cd}\cos\varphi_R(\grave{r}),\omega|\grave{r})\mathrm{e}^{\mathrm{i}j\sigma}\mathrm{e}^{\mathrm{i}k_{z_{c0}}\sin\varphi_R x_{cd}}\,\mathrm{d}k_{z_{\mathrm{R}0}}\,\mathrm{d}k_{x_d}. \tag{28}$$

Eqs. (12b), (23) and (28) yield the cross-spectrum of the unsteady blade loadings:

$$\begin{aligned} S^{(jj')}_{\mathrm{FF},cd}(x_{cd},r,\omega;x'_{cd},r',\omega') = \frac{(\rho_0 c_0 w_{\mathrm{rms,b}}(\grave{r}))^2}{rU_{x_d}(\grave{r})}\sum_{m_g\in\mathbb{Z}}\int \mathrm{e}^{-\mathrm{i}k_{z_{\mathrm{R}0}}\Delta r}\mathrm{e}^{-\mathrm{i}2\pi((j-j')/B_R)m_g}\times\Phi_{\mathrm{ww,b}}(\mathbf{K}_{\mathrm{R}0},\grave{r})\mathrm{e}^{\mathrm{i}k_{z_{c0}}[\sin\varphi_R(\grave{r})x_{cd}-\sin\varphi_R(\grave{r}')x'_{cd}]}\\ \times\delta(\omega'-\omega)\Delta\widehat{P}_{c,0}(x_{cd}\cos\varphi_R(\grave{r})|m_g,k_{z_{\mathrm{R}0}},\omega,\grave{r})\\ \times\Delta\widehat{P}_{c,0}(x'_{cd}\cos\varphi_R(\grave{r}')|m_g,k_{z_{\mathrm{R}0}},\omega,\grave{r}')^*\mathrm{d}k_{z_{\mathrm{R}0}}, \end{aligned} \tag{29a}$$

where $\Delta\widehat{P}_{c,0}(x_{cd}\cos\varphi_R(\grave{r})|m_g,k_{z_{\mathrm{R}0}},\omega,\grave{r}) \equiv \Delta\widehat{P}_{c,0}(x_{cd}\cos\varphi_R(\grave{r}),\omega|\grave{r})$ to refer to the incident gust azimuthal order m_g and to the radial wavenumber $k_{z_{\mathrm{R}0}}$ and $\Delta r = r - r'$. The axial wavenumber $k_{x_{\mathrm{R}0}}$ of wavenumber vector in the duct frame of reference $\mathbf{K}_{\mathrm{R}0}$, defined in Eq. (23), is set equal to

$$k_{x_{\mathrm{R}0}} = \frac{\omega + m_g\Omega_R}{U_{x_d}(\grave{r})}. \tag{29b}$$

The wavenumber in the cascade frame of reference is $\mathbf{K}_{c0} = \mathbf{Q}\cdot\mathbf{K}_{\mathrm{R}0}$ with in particular:

$$k_{z_{c0}} = Q_{31,\mathrm{R}}\frac{\omega}{U_{x_d}(\grave{r})} - \frac{m_g}{r}[Q_{32,\mathrm{R}} - \tan\check{\chi}_R Q_{31,\mathrm{R}}] + Q_{33,\mathrm{R}}k_{z_{\mathrm{R}0}}, \tag{30}$$

from Eq. (A.13) in Appendix A.2.1.

2.2.3. Power spectral density of the acoustic power

Eq. (29a) of the cross-spectrum of the unsteady blade loadings combined with Eq. (12a) finally gives the expected value of the spectrum of the duct mode (m,μ):

$$\begin{aligned} \lim_{T\to\infty}\frac{\pi}{T}E[|\mathcal{P}_{m,\mu}(\omega)|^2] = \left(\frac{B_R\rho_0 c_0}{2|\kappa_{m\mu}|\Gamma_{m\mu}}\right)^2\int_{R_H}^{R_T}\frac{w_{\mathrm{rms,b}}(\grave{r})^2 S^{\pm}_{m,\mu}(\grave{r},\omega)}{rU_{x_d}(\grave{r})}\int_{-L_r}^{L_r} S^{\pm}_{m,\mu}(\grave{r}+\Delta\grave{r},\omega)^*\sum_{m_g\in\mathbb{Z}}\sum_{k\in\mathbb{Z}}\delta_{m,m_g+kB_R}\int\Phi_{\mathrm{ww,b}}(\mathbf{K}_{\mathrm{R}0},\grave{r})\\ \times I_{c,m,\mu}(\grave{r},\omega,m_g,k_{z_{\mathrm{R}0}})I_{c,m,\mu}(\grave{r}+\Delta\grave{r},\omega,m_g,k_{z_{\mathrm{R}0}})^*\mathrm{e}^{-\mathrm{i}k_{z_{\mathrm{R}0}}\Delta r}\,\mathrm{d}k_{z_{\mathrm{R}0}}\\ \times\mathrm{e}^{-\mathrm{i}(m/(r+\Delta r))y_{LE,R}(\grave{r}+\Delta\grave{r})+\mathrm{i}k^{\pm}_{x_R,m\mu}x_{LE,d}(\grave{r}+\Delta\grave{r})}\,\mathrm{d}\Delta r\times\mathrm{e}^{\mathrm{i}(m/r)y_{LE,R}(\grave{r})-\mathrm{i}k^{\pm}_{x_R,m\mu}x_{LE,d}(\grave{r})}\,\mathrm{d}r, \end{aligned} \tag{31a}$$

with

$$I_{c,m,\mu}(\grave{r},\omega,m_g,k_{z_{\mathrm{R}0}}) = \int_0^{c_d(r)}\Delta\widehat{P}_{c,0}(x_{cd}\cos\varphi_R(\grave{r})|m_g,k_{z_{\mathrm{R}0}},\omega_m,\grave{r})\mathrm{e}^{\mathrm{i}[k_{z_{c0}}\sin\varphi_R(\grave{r})-k^{\pm}_{x'_{cd},m\mu}(r)]x_{cd}}\,\mathrm{d}x_{cd}. \tag{31b}$$

The summation over k with the Kronecker symbol results from the double summation over the blade indices j and j'. This leads to the condition $m - m_g \equiv 0 \pmod B$ corresponding to Tyler and Sofrin's condition [56]. This formulation neglects the difference of radii r and r' in the amplitude of the gust $w_{\mathrm{rms,b}}$, in the factor $\rho_0 c_0$, and in the wavenumber along y_d ($-m_g/r$ and $-m'_g/r$) in the three-dimensional spectrum. But the radii are kept different in the duct functions, in the calculation of the cascade response function and in the phase terms. A further simplification is introduced now to avoid the numerical integration in Δr which is both time consuming and error-prone. Eq. (31a) is simplified by assuming that the radial distance $\Delta r = r' - r$ on which the blade loads are correlated is small compared to the duct height $R_T - R_H$. The difference of radii is retained only in the phase terms and neglected in the amplitude terms, as proposed by Glegg and Jochault [57]. The eigenfunction $E_{m,\mu}$ can be expressed as a linear combination of two Hankel functions of first and second kinds as

$$E_{m,\mu}(r) = C_{m,\mu}H^{(1)}_m(\chi_{m,\mu}r) + D_{m,\mu}H^{(2)}_m(\chi_{m,\mu}r). \tag{32}$$

If a Taylor expansion of the Hankel functions is made around r, and the variation of $\zeta^{\pm}_{m,\mu}$ in Δr is neglected, the duct function $S^{\pm}_{m\mu}$ takes the approximate form

$$S^{\pm *}_{m,\mu}(r',\omega)^{\pm} \simeq \zeta^{\pm *}_{m,\mu}(r)C^*_{m,\mu}H^{(1)*}_m(\chi_{m,\mu}r)\mathrm{e}^{-\mathrm{i}k^*_{z_{d1}}\Delta r} + \zeta^{\pm *}_{m,\mu}(r)D^*_{m,\mu}H^{(2)*}_m(\chi_{m,\mu}r)^*\mathrm{e}^{\mathrm{i}k_{z_{d1}}\Delta r} \tag{33a}$$

with

$$k_{z_{d1}} = -i\frac{\mathrm{d}}{\mathrm{d}r}(\ln(H^{(1)}_m(\chi_{m,\mu}r))) = -\mathrm{i}\frac{\chi_{m,\mu}H^{(1)\prime}_m(\chi_{m,\mu}r)}{H^{(1)}_m(\chi_{m,\mu}r)} = -\mathrm{i}\left(\frac{\chi_{m,\mu}H^{(2)\prime}_m(\chi_{m,\mu}r)}{H^{(2)}_m(\chi_{m,\mu}r)}\right)^*, \tag{33b}$$

In addition, the variations of the cascade response function $\Delta\widehat{P}_{c,0}$ with the radius in the interval Δr are also neglected. This is valid if the cascade geometry can be assumed unchanged over the radial correlation length l_r (assumption **H4**). But, the

variation is kept in the phase term γ:

$$\gamma(r,r') = (k_{z_{c0}}\sin\varphi_R(\grave{r}) - k^{\pm}_{x_{cd},m\mu}(\grave{r}))x_{cd} - (k_{z_{c0}}\sin\varphi_R(\grave{r}') - k^{\pm}_{x_{cd},m\mu}(\grave{r}'))x'_{cd} - k_{z_{R0}}\Delta r - \frac{m}{r'}y_{\mathrm{LE,R}}(\grave{r}') + k^{\pm}_{x_R,m\mu}x_{\mathrm{LE,d}}(\grave{r}') + \frac{m}{r}y_{\mathrm{LE,R}}(\grave{r}) - k^{\pm}_{x_R,m\mu}x_{\mathrm{LE,d}}(\grave{r}). \tag{34}$$

It can be simplified from assumption **H4** as

$$\gamma(r,r') = (k_{z_{c0}}\sin\varphi_R(\grave{r}) - k^{\pm}_{x_{cd},m\mu}(\grave{r}))(x_{cd}-x'_{cd}) + \left[-k_{z_{R0}} - \frac{m\tan\check{\psi}_R(\grave{r})}{r} + k^{\pm}_{x_R,m\mu}\tan\check{\varphi}_R(\grave{r})\right]\Delta r. \tag{35}$$

Introducing the wavenumbers:

$$K_1 = -k^{*}_{z_{d1}} + k^{\pm}_{x_R,m\mu}\tan\check{\varphi}_R - \frac{m}{r}\tan\check{\psi}_R,$$

$$K_2 = k_{z_{d1}} + k^{\pm}_{x_R,m\mu}\tan\check{\varphi}_R - \frac{m}{r}\tan\check{\psi}_R, \tag{36}$$

the PSD of the amplitude of the duct mode (m,μ) is expressed as

$$\langle|\mathcal{P}^{\pm}_{m,\mu}(\omega)|^2\rangle = \left(\frac{B_R\rho_0 c_0}{2|\kappa_{m\mu}|\Gamma_{m\mu}}\right)^2 \int_{R_H}^{R_T} \frac{w_{\mathrm{rms,b}}(\grave{r})^2 S^{\pm}_{m,\mu}(\grave{r},\omega)}{rU_{x_d}(\grave{r})}\zeta^{\pm *}_{m,\mu}(\grave{r},\omega)\sum_{m_g\in\mathbb{Z}}\sum_{k\in\mathbb{Z}}\delta_{m,m_g+kB_R}\int \Phi_{\mathrm{ww,b}}(\mathbf{K}_{\mathrm{R0}},\grave{r}) \times[C^{*}_{m,\mu}H^{(1)*}_{m}(\chi_{m,\mu}r)\mathrm{Int}(\grave{r},K_1) + D^{*}_{m,\mu}H^{(2)*}_{m}(\chi_{m,\mu}r)\mathrm{Int}(\grave{r},K_2)]|Idp_{c,m,\mu}(\grave{r},\omega,m_g,k_{z_{R0}})|^2 \mathrm{d}k_{z_{R0}}\,\mathrm{d}r, \tag{37a}$$

where

$$\mathrm{Int}(\grave{r},K_i) = \int_{-L_r}^{+L_r} \mathrm{e}^{\mathrm{i}[K_i - k_{z_{R0}}]\Delta r}\,\mathrm{d}\Delta r = 2L_r\,\mathrm{sinc}([K_i - k_{z_{R0}}]L_r). \tag{37b}$$

The PSD of the acoustic power is finally given by Eq. (5a). The accuracy of the simplification will be investigated as a function of the frequency and the duct mode orders in Section 3.2.4.

2.3. Impingement of wake and background turbulence on OGV

2.3.1. Statistical properties of the turbulence

Since the incident disturbance on the stator corresponds to the turbulence downstream of the rotor, its properties are introduced in the rotor rotating frame of reference $\mathcal{R}_R$. The upwash velocity then reads

$$\mathbf{u}(\mathbf{x}_R,t)\cdot\mathbf{n}_c = w(\mathbf{x}_R,t) = \check{w}(\mathbf{x}_R - tU_{x_d}\mathbf{e}_{x_d}), \tag{38}$$

instead of Eq. (13).

As proposed by Nallasamy and Envia [17], the turbulence is split into the sum of a background component (subscript b) and a component from the turbulent rotor wakes (subscript w) which is assimilated to a random term multiplied by a deterministic envelope ϑ though possibly controversial this choice is made for a more relevant comparison of the present results with the reference. The assumption of locally homogeneous turbulence allows writing

$$w(\mathbf{x}_R,t) = w_b(\mathbf{x}_R,t) + w_w(\mathbf{x}_R,t) = \check{w}_b(\mathbf{x}_R - tU_{x_d}(\grave{r})\mathbf{e}_{x_d}) + \check{w}_w(\mathbf{x}_R - tU_{x_d}(\grave{r})\mathbf{e}_{x_d}) \tag{39a}$$

with

$$\check{w}_b(\mathbf{x}_R) = w_{\mathrm{rms,b}}(\grave{r})\overline{w}_b(\check{\mathbf{x}}_R|\grave{r}) \quad\text{and}\quad \check{w}_w(\mathbf{x}_R) = w_{\mathrm{rms,w}}(\grave{r})\vartheta(\mathbf{x}_R\cdot\mathbf{n}_R)\overline{w}_w(\check{\mathbf{x}}_R|\grave{r}). \tag{39b}$$

Again, the symbols above the coordinates are only to remind that the amplitudes $w_{\mathrm{rms,i}}$ and integral length scales $(l_{a,i},l_{t,i})$ or Λ_{i} of the turbulence (i = b or w) vary with the reference radius r but that the turbulence itself is nearly isotropic or homogeneous and axisymmetric in the vicinity of this radius. Then a Liepmann or an axisymmetric turbulence model is involved to describe the spectrum of the non-dimensional velocities $\overline{w}_i(\check{\mathbf{x}}_R,\grave{r})$, i = b or w. The envelope ϑ is taken to be a periodic series of Gaussian profiles as proposed by Nallasamy and Envia [17], each one corresponding to the wake downstream of a particular blade:

$$\vartheta(x_R,y_R) = \sum_{j\in\mathbb{Z}}\exp\left(-\pi\left[\frac{y_R - x_R\tan(\chi_R(\grave{r})) - jg_R(\grave{r})}{L_w}\right]^2\right) = \vartheta(\mathbf{x}_R\cdot\mathbf{n}_R) = \sum_{j\in\mathbb{Z}}\exp\left(-\pi\left[\frac{\mathbf{x}_R\cdot\mathbf{n}_R(\grave{r}) - jg_R(\grave{r})\cos(\chi_R)}{\cos(\chi_R)L_w}\right]^2\right). \tag{40}$$

$g_R(\grave{r}) = 2\pi r/B_R$ is the pitchwise distance between two successive rotor blades in the duct section and L_w the width of the wakes. This has been shown to be a very good approximation for broadband noise predictions [58]. The distribution being

$[g_R \cos\chi_R(\dot{r})]$-periodic, it can be expanded in Fourier series:

$$\vartheta(\mathbf{x}_R \cdot \mathbf{n}_R(\dot{r})) = \sum_{n\in\mathbb{Z}} \vartheta_n(\dot{r}) \mathrm{e}^{-\mathrm{i}nB_R \mathbf{x}_R \cdot \mathbf{n}_R(\dot{r})/r\cos\chi_R(\dot{r})} \tag{41a}$$

with

$$\vartheta_n(\dot{r}) = \frac{L_w(\dot{r})}{g_R(\dot{r})} \mathrm{e}^{-\pi(nL_w(\dot{r})/g_R(\dot{r}))^2} \tag{41b}$$

As previously, $\check{w}$ and w are periodic functions of the azimuthal angle.

In addition, since the turbulence interacts with the stator, the cross-spectrum of the upwash velocity must be given in the stator frame of reference $\mathcal{R}_S$ which leads to the Fourier transform:

$$w_{m_g}(k_{x_S}, k_{z_{S0}}, \omega) = \frac{1}{(2\pi)^4} \iiint_{\mathbb{R}^3} \int_{-\pi}^{\pi} w(\mathbf{x}_R, t) \mathrm{e}^{\mathrm{i}\omega t + \mathrm{i}k_{x_S} x_S - \mathrm{i}m_g\theta_S - \mathrm{i}k_{z_{S0}} r} \,\mathrm{d}\theta_S \,\mathrm{d}r \,\mathrm{d}x_S \,\mathrm{d}t. \tag{42}$$

Again, the expected value of the turbulent inflow wavenumber frequency spectrum can be expressed as

$$S_{\mathrm{WW}} = \sum_{m_g\in\mathbb{Z}} \sum_{m'_g\in\mathbb{Z}} S_{\mathrm{WW}}^{m_g, m'_g} \tag{43a}$$

with

$$S_{\mathrm{WW}}^{m_g, m'_g} = \langle w_{m_g}(k_{x_S}, k_{z_{S0}}, \omega) w_{m'_g}(k'_{x_S}, k'_{z_{S0}}, \omega')^* \rangle. \tag{43b}$$

This expected value of the turbulent inflow wavenumber frequency spectrum of modes m_g and m'_g is the sum of the three terms corresponding to the background turbulence $S_{\mathrm{WW,b}}^{m_g, m'_g}$, the wake turbulence $S_{\mathrm{WW,w}}^{m_g, m'_g}$ contributions and the background/wake cross-correlation $S_{\mathrm{WW,bw}}^{m_g, m'_g}$. The latter is set equal to zero by assuming that the background turbulence and the turbulence in the wakes are not correlated. After some algebra, and a change from the rotating frame of reference fixed to the rotor $\mathcal{R}_R$ to a stationary frame of reference attached to the diffracting stator cascade $\mathcal{R}_S$ — in a rather similar way as above — the upwash expected value of the background turbulence $S_{\mathrm{WW,b}}$ is written as

$$\begin{aligned} S_{\mathrm{WW,b}}^{m_g, m'_g} &= \langle w_{\mathrm{b},m_g}(k_{x_S}, k_{z_{S0}}, \omega) w_{\mathrm{b},m'_g}(k'_{x_S}, k'_{z_{S0}}, \omega')^* \rangle \\ &= \frac{w_{\mathrm{rms,b}}(\dot{r})^2}{r} \delta(\omega - k_{x_{S0}} U_{x_d}(\dot{r}) + m_g U_\theta / r) \delta(\omega' - \omega) \delta(k_{x_{S0}} - k'_{x_{S0}}) \delta_{m_g, m'_g} \delta(k_{z_{S0}} - k'_{z_{S0}}) \Phi_{\mathrm{ww,b}}(\mathbf{K}_{S0}, \dot{r}) \end{aligned} \tag{44}$$

where $\Phi_{\mathrm{ww,b}}$ is the PSD of $\overline{w}_b$, and

$$\mathbf{K}_{S0} = \left(k_{x_{S0}}, -\frac{m_g}{r}, k_{z_{R0}}\right) \tag{45}$$

with $k_{x_{S0}} = -k_{x_S}$. This result is the analogue of Eq. (23) in the rotating case. It also supposes that the radial integral length scale is small compared with the radial variation of the excitation, i.e. that the two radii can be taken equal in the amplitude terms. In a same way, the cross-correlation of wake turbulence $S_{\mathrm{WW,w}}^{m_g, m'_g}$, can be derived as

$$\begin{aligned} S_{\mathrm{WW,w}}^{m_g, m'_g} = \frac{w_{\mathrm{rms,w}}(\dot{r})^2}{r} \sum_{n_1\in\mathbb{Z}} \vartheta_{n_1}(\dot{r}) \sum_{n_2\in\mathbb{Z}} \vartheta_{n_2}(\dot{r})^* \delta(\omega' - \omega - (n_1 - n_2) B_R \Omega_R) \delta\left(\omega + \frac{m_g}{r} U_\theta - k_{x_{S0}} U_{x_d}(\dot{r})\right) \mathrm{e}^{-\mathrm{i}(((n_1-n_2)B_R)/r)\tan\chi_R(\dot{r}) D_{\mathrm{RS}}} \\ \times \Phi_{\mathrm{ww,w}}\left(k_{x_{S0}} - \frac{n_1 B_R \tan\chi_R(\dot{r})}{r}, -\frac{m_g - n_1 B_R}{r}, k_{z_{R0}}, \dot{r}\right) \delta(k'_{z_{S0}} - k_{z_{S0}}) \\ \times \delta\left(k_{x_{S0}} - k'_{x_{S0}} - \frac{(n_1 - n_2) B_R}{r} \tan\chi_R(\dot{r})\right) \delta_{m_g, m'_g - (n_1 - n_2) B_R} \end{aligned} \tag{46}$$

2.3.2. Power spectral density of the acoustic power

The PSD of the amplitude of the duct mode (m,μ) is as in Section 2.2. It can be approximated by the expression

$$\begin{aligned} \langle |\mathcal{P}_{m,\mu}^{\pm}(\omega)|^2 \rangle = \left(\frac{B_S \rho_0 c_0}{2|\kappa_{m\mu}|\Gamma_{m\mu}}\right)^2 \int_{R_H}^{R_T} \frac{S_{m,\mu}^{\pm}(\dot{r},\omega) \zeta_{m,\mu}^{\pm *}(\dot{r},\omega)}{r U_{x_d}(\dot{r})} \sum_{m_g\in\mathbb{Z}} \sum_{k\in\mathbb{Z}} \delta_{m, m_g + kB_S} \int \Big[w_{\mathrm{rms,b}}(\dot{r})^2 \Phi_{\mathrm{ww,b}}(\mathbf{K}_{S0}, \dot{r}) \\ + w_{\mathrm{rms,w}}(\dot{r})^2 \sum_{n_1\in\mathbb{Z}} |\vartheta_{n_1}(\dot{r})|^2 \Phi_{\mathrm{ww,w}}(\tilde{\mathbf{K}}_{S0}(n_1), \dot{r}) \Big] \\ \times [C_{m,\mu}^* H_m^{(1)*}(\chi_{m,\mu} r) \mathrm{Int}(\dot{r}, K_1) + D_{m,\mu}^* H_m^{(2)*}(\chi_{m,\mu} r) \mathrm{Int}(\dot{r}, K_2)] \\ \times |I dp_{c,m,\mu}(\dot{r}, \omega, m_g, k_{z_{S0}})|^2 \,\mathrm{d}k_{z_{S0}} \,\mathrm{d}r, \end{aligned} \tag{47a}$$

where $\mathrm{Int}(\grave{r},K_i)$ is defined in Eq. (37b),

$$\mathbf{K}_{S0}=\left(\frac{\omega-k_{y_{S0}}U_\theta(\grave{r})}{U_{x_d}(\grave{r})},-\frac{m_g}{r},k_{z_{S0}}\right) \tag{47b}$$

and

$$\tilde{\mathbf{K}}_{S0}(n_1)=\left(\frac{\omega+n_1B_R\Omega_R}{U_{x_d}(\grave{r})}+\frac{m_g-n_1B_R}{r}\tan\chi_S(\grave{r}),-\frac{m_g-n_1B_R}{r},k_{z_{S0}}\right), \tag{47c}$$

similarly to Eq. (37a) in the case of the rotor in Section 2.2. The PSD of the acoustic power is finally given by Eq. (5a).

2.4. Definition of the length scale L_r

An important input to the model is the radial correlation length of the unsteady blade loading $l_r\equiv 2L_r$, which is almost neither measured nor computed. Even though the recent measurements by Envia [40] seem to show that the unsteady blade loading is likely correlated over a longer distance than the incident velocity, l_r is usually assimilated to the radial correlation length of the incident, locally isotropic or axisymmetric homogeneous turbulence, as usually done for the broadband noise due to the interaction of an incident turbulence with an isolated airfoil [59]. l_r is then defined as the radial correlation length relating the two-dimensional spectrum of the upwash velocity $\widehat{\Phi}_{ww}(k_{x_c},k_{z_c})$ in $(k_{x_c},k_{z_c})=(\omega/U_0,0)$ to the PSD of the upwash velocity $\breve{\Phi}_{\mathrm{ww}}(\omega)$, by the relation

$$\widehat{\Phi}_{\mathrm{ww}}\left(\frac{\omega}{U_0},0\right)=\frac{U_0}{\pi}l_r(\omega)\breve{\Phi}_{\mathrm{ww}}(\omega), \tag{48}$$

given by Hinze [60] and used by Amiet [59], where U_0 is the mean flow velocity. The two-dimensional spectrum is obtained by integration of the three-dimensional spectrum Φ_{ww} over the wavenumber along the normal of the blade k_{y_c}.

2.5. Turbulence models

The three-dimensional spectrum of the upwash velocity of the locally homogeneous turbulence Φ_{ww} and the radial correlation length l_r of the upstream turbulence are the properties of the upstream turbulence needed as input data. The inlet turbulence is assumed locally isotropic and homogeneous according to Liepmann's model [61] or a Gaussian model (see Appendix C.1). Von Kármán's model [60] could have been used instead but is not presented here for conciseness. When not mentioned Liepmann's model is used. The isotropy of turbulence is typical of well-controlled wind-tunnel experiments and fan test rigs. In contrast, the turbulence in the annulus of a turbomachinery is hardly isotropic as outlined by Kerschen and Gliebe [62]. For instance, the eddies of ingested turbulence are often elongated in the axial direction upstream of the rotor in static test conditions [63]. In the present study, to assess the effect of anisotropy, locally homogeneous and axisymmetric turbulence is also investigated. It should be closer to the actual turbulence in a turbofan duct in particular for a rotor in static condition (mostly for the rotor ingestion noise but also for the stator interaction noise). In normal flight condition, the ingested turbulence is mostly isotropic; however possible anisotropy may be observed in the turbulent rotor wakes. It will also allow studying the importance of an accurate definition of the turbulence impinging a blade row on the broadband noise prediction. The physically consistent model developed by Kerschen and Gliebe [62] is considered. It is based on the earlier works by Batchelor [64] and Chandrasekhar [65,66]. Kerschen and Gliebe [62] reviewed the first analyses of anisotropic turbulence, from Hanson's model of discrete eddies with random properties [63] to Mani [67] and Mani and Bekofske [68]'s work resorting to the description of turbulence in a contraction stream by Ribner and Tucker [69]. This rapid distortion theory [69,70] could have been used here as was done by Atassi and Logue [71]. However, as outlined by Kerschen and Gliebe [62] a too large ratio of velocities u_t/u_a (e.g. from Eqs. (34) and (35) of [69], $u_t/u_a=4.9$ for $l_a=5\Lambda$ and $l_t=\Lambda/\sqrt{5}$) is induced for a realistic value of the ratio of the axial and transverse length scales l_a/l_t. The expressions of the three-dimensional spectrum Φ_{ww} and the correlation length l_r for the axisymmetric model of Kerschen and Gliebe are derived in Appendix C.2.

2.6. Correction in the vicinity of the cut-on frequencies

A correction of the model has been introduced in the vicinity of the duct modes cut-on frequencies as proposed by Posson and Roger [39] to avoid unrealistic peak response. The peaks are found because of the non-coincidence of the cut-on frequencies of the annular duct modes and the cut-on frequencies of the rectilinear cascade obtained when unwrapping an annular strip. Posson and Roger [39] enforced the coincidence by choosing a particular gust spanwise-wavenumber $k_{z_{c0}}$ when the azimuthal order of the gust $m_g\equiv m\ (\mathrm{mod}\ B_l)$ and the angular frequency ω is close to the cut-on frequency of the duct mode of azimuthal order m. They showed a substantial reduction of most of these unrealistic peaks in the rather low-frequency experiment performed on a stator annular cascade briefly described in the next section.

2.7. Annular effect: correction of the unsteady blade loading formulation

The unsteady blade loading for a rectilinear-cascade model was derived by Posson et al. [35] based on Glegg's model [21]. To evaluate the accuracy of the strip-theory approach, the category 4 of the Third Computational Aeroacoustic benchmark [72] has been investigated [73,34]. Narrow and moderate annular cascades are excited by a mean rotor-wake harmonic. The unsteady blade loading produced by the rectilinear-cascade model [34], the unsteady pressure field in the blade passage [73] and the radiated acoustic duct modes [34] (produced by applying the acoustic analogy in an annular duct with the unsteady blade loading as equivalent dipole sources) were compared with the results of more accurate three-dimensional numerical methods. Some discrepancies were only found in the prediction of the unsteady blade loading and consequently on the acoustic field for annulus with a small hub-to-tip ratio. A comparison of the dispersion relation in an annular duct and a rectilinear configuration highlighted the presence of additional terms in the annular case, caused by annular effects. A correction of the rectilinear-cascade model and hence of the unsteady blade loading was then detailed [34]. The results suggested that this correction is necessary to get closer to the underlying physics of the annular-space wave equation, but still remain significantly different from the three-dimensional results. Better results should be expected in the present broadband case. The correction which mainly consists in introducing a corrected radial wavenumber is then introduced in the current model and its effect on the results will be discussed in the next validation section.

2.8. Concluding remarks: summary of the model

As outlined at the beginning of the section, the model can be considered as an extension of Ventres et al. [16] as it uses an acoustic analogy in an annular duct with uniform mean flow, and a cascade response function to compute the unsteady blade loading. Nevertheless, three important differences have been highlighted.

Firstly, the unsteady blade response used in each strip is a three-dimensional response which accounts for three-dimensional incident gusts and which can deal with a more general blade row involving both non-zero sweep and lean angles. Indeed, even if the radial variations of the geometry and of the mean flow features and turbulence are treated as parametric variations, the local three-dimensionality of the turbulence is introduced in the unsteady blade response function. Moreover, the effect of the first subcritical gusts is introduced.

Secondly, considering the three-dimensional turbulence spectra permits to introduce a non-zero radial correlation length l_r, and as a result, the cross-correlation of the unsteady blade loading for two close but not identical radial positions. Indeed, former works of Ventres et al. [16] or Nallasamy and Envia [17] assume that the radial integral length scale is very small compared to the duct radius and then neglect the difference of radii in all terms except in the turbulence correlation function which ends in exhibiting the radial integral length scale as a multiplicative factor of the solution.

Thirdly, the formulation has been written in cylindrical coordinates to reckon with the annular geometry and its effect on turbulence, instead of using Cartesian coordinates.

Finally, several turbulence models are investigated. The main interest of this last point is to quantify the effect of the turbulence model on the broadband noise prediction (Section 3.4).

3. Fan-OGV broadband noise predictions

3.1. Experimental data and preliminary assessment

In order to assess the model, Posson and Roger [39] proposed a dedicated experiment in a subsonic anechoic wind-tunnel facility. The experimental set-up has been designed to isolate the noise due to the interaction of an incident turbulent flow with a stationary annular cascade of vanes as much as possible. The cascade has 49 or 98 vanes of 25 mm chord length, a tip radius of 230 mm, and a hub-to-tip ratio of 0.65. The mean velocity ranges from 50 m/s to 100 m/s. A turbulence-generating grid is inserted upstream to ensure a turbulent intensity of about 5.5 percent. As a result, the test case corresponds to a low-frequency turbomachinery problem with relatively few cut-on duct modes. The resulting broadband noise was predicted with the model described in Section 2.2 for the noise produced by a background turbulence impinging on a blade row. Despite spurious numerical peaks, the predictions were found to differ by less than 2 dB from the experimental data and reproduced the proper trend between the two annular cascades. Yet this was still far from a realistic fan configuration involving more modes and a rotor/stator stage. For a more convincing validation, the model must be assessed also in the case of rotor wakes interacting with stator vanes. This is achieved here with the experimental results of the 22-in source diagnostic test (SDT) fan rig of NASA Glenn's 9×15 low-speed wind tunnel [40–46,15]. The SDT experiments were performed on a fan stage composed of 22 rotor blades and three different OGV: the baseline OGV with 54 radial vanes, the low-count OGV with 26 radial vanes and the low-noise OGV with 26 swept vanes. Three flight conditions were investigated : approach, cut-back and fly-over. Both the flow field and the acoustic field were measured. The comparison is performed for the two radial OGV in the approach configuration, for which the main characteristics are summarized in Table 1 [17,42,74]. The duct dimensions lead to about 2600 and 4600 cut-on modes at 30 and 40 kHz respectively. For the numerical assessment of the present broadband noise model, the baseline configuration only is used, in Sections 3.2 and 3.3. The low-count configuration is then used to assess the effect of the incident turbulence in Section

Table 1
Main geometrical and aerodynamic parameters of the studied SDT cases.

B_R	R_H/R_H	R_T (m)	Ω_R (rad s^{-1})	T_0 (K)	ρ_0 (kg m^{-3})	
22	0.5	0.28	817.65	288	1.248	
OGV	B_S	c (m)	$\chi(R_H)$ (deg)	$\chi(R_m)$ (deg)	$\chi(R_T)$ (deg)	
Baseline	54	0.04	35.9	29.8	33.1	
Low-count	26	0.082	33.5	29.7	33.1	
OGV	$U_{x_d}(R_H)$ (m s^{-1})	$U_{x_d}(R_m)$ (m s^{-1})	$U_{x_d}(R_T)$ (m s^{-1})	$U_\theta(R_H)$ (m s^{-1})	$U_\theta(R_m)$ (m s^{-1})	$U_\theta(R_T)$ (m s^{-1})
Baseline	105.9	111.1	71.1	102.2	75.9	80.0
Low-count	107.1	115.8	66.6	101.6	75.0	71.4
OGV	$\Lambda(R_H)$ (m)	$\Lambda(R_m)$ (m)	$\Lambda(R_T)$ (m)	$L_w(R_H)$ (m)	$L_w(R_m)$ (m)	$L_w(R_T)$ (m)
Baseline	0.0046	0.0058	0.013	0.036	0.049	0.088
Low-count	0.0054	0.0061	0.014	0.020	0.026	0.040
OGV	$u_{\mathrm{rms},b}(R_H)$ (m s^{-1})	$u_{\mathrm{rms},b}(R_m)$ (m s^{-1})	$u_{\mathrm{rms},b}(R_T)$ (m s^{-1})	$u_{\mathrm{rms},w}(R_H)$ (m s^{-1})	$u_{\mathrm{rms},w}(R_m)$ (m s^{-1})	$u_{\mathrm{rms},w}(R_T)$ (m s^{-1})
Baseline	4.62	2.90	9.13	0.15	4.86	0.97
Low-count	4.22	2.72	10.55	0.44	5.11	0.50

3.4. Both configurations are considered in the final validation of the model in Section 3.5. Moreover, the model is also compared with the predictions of Nallasamy and Envia [17] in this final section. It is important to highlight that the acoustic power predicted by the model assumes an infinite duct whereas experimental acoustic power is computed from measurements outside of the duct. The reflexion at the duct end and the diffraction by the shear layers notably can modify the overall power as well as the frequency content. Besides the presence of the rotor in the experiment introduces a shielding effect, a coupling between the blade rows and a swirling mean flow in between the rotor and the stator. All these aspects may considerably modify the response. Finally, the experimental measurements and the blade row manufacturing process can introduce additional uncertainties in the experimental results. All these differences and uncertainties will have to be kept in mind when assessing the model. For instance an exact agreement in level will not mean a perfect prediction by the model but rather a very good agreement.

Besides, before any comparison, it is necessary to verify that the domain of validity of the cascade model contains the studied frequency range. The low-frequency limit of the model is specified by the numerical truncation of the infinite matrix system coupling the leading edges and trailing edges in the rectilinear-cascade model, since Glegg's cascade response function [21] gives the exact solution for an infinitely thin flat-plate cascade of finite length. However, using Richardson's procedure together with 100 terms in the matrix gives well converged results. The good accuracy well below the low-frequency limit of a two-steps Schwarzschild procedure has already been outlined in the limit case of a reduced cascade effect [35], with an agreement for $k_1 = \omega c/(2U_c) > 2$ in the incompressible case. Compressibility effects and cascade effects may modify this limit, in the present configuration. However, the model has been shown in a good agreement with experimental data in the case of an isolated stator impinged by a turbulent flow [39] for $k_1 > 0.6$ (600 Hz in [39]). The low-frequency range [1,2] kHz ($k_1 \in [1,2]$) will then have to be considered more carefully.

3.2. Numerical assessment of the model

The numerical evaluations of the integral over $\mathbb{R}$ and series involved in the model require truncations. The truncation criteria and their effects are studied in Section 3.2.1 for the integration in spanwise wavenumber and in Section 3.2.2 for the series in azimuthal order of the incident perturbation m_g.

3.2.1. Convergence of the numerical integration in the spanwise wavenumber

Results below are obtained for $m_g \in [-N_{m_g}, N_{m_g}]$ with $N_{m_g} = 200$. The integration on the radial wavenumber $k_{z_{s0}}$ over $\mathbb{R}$ and then the spanwise wavenumber $k_{z_{c0}}$ over $\mathbb{R}$ is performed numerically by integrating over a particular range $[k_{z_{c0,\min}}, k_{z_{c0,max}}]$. It is first possible to determine the maximal and minimal values of the spanwise wavenumber such that at least one cascade radiation mode propagates outside, namely the cascade is cut-on for this gust. These values are defined by

$$k_{z_{c0,\max,\mathrm{crit.}}} = \max_{k\in\mathbb{Z}}(k_{z_{c0,\mathrm{crit.}}}(k)) = \frac{\omega_{\mathrm{ex}}}{(\beta + M_w)c_0}\,, \tag{49a}$$

and

$$k_{z_{c0,\min,\text{crit.}}} = \min_{k\in\mathbb{Z}}(k_{z_{c0,\text{crit.}}}(k)) = \frac{-\omega_{\text{ex}}}{(\beta - M_w)c_0}, \tag{49b}$$

where k is a cascade diffraction order, and $k_{z_{c0,\text{crit.}}}(k)$ is the spanwise wavenumber for which the cascade mode k goes from cut-on to cut-off. The cut-on condition of the mode k for $k_{z_{c0}}$ reads

$$-\frac{[\beta_w^2 s^2 - (Mh)^2]}{\beta^2 s_e^2}k_{z_{c0,\text{crit.}}}^2 + 2M_w\left(\left[\sigma - 2\pi k + \frac{\omega_{\text{ex}} Md}{\beta^2 c_0}\right]\frac{Md}{\beta^2 s_e^2} - \frac{\omega_{\text{ex}}}{\beta^4 c_0}\right)k_{z_{c0,\text{crit.}}} + \frac{\omega_{\text{ex}}^2}{\beta^4 c_0^2} - \frac{1}{s_e^2}\left(\sigma - 2\pi k + \frac{\omega_{\text{ex}} Md}{\beta^2 c_0}\right)^2 = 0, \tag{50}$$

where d, h, s, M, β, s_e and β_w are defined in Appendix B. The two bounds of Eq. (49b) correspond to the bounds of the ellipse outlined by Hanson [22] [22, Fig. 10] in the rectilinear model. However, the problem is posed in a different way here. Indeed, the sound radiated on a particular duct mode m by an incident gust of azimuthal order m_g is computed from the unsteady blade loading produced by this gust. The loading contains a summation over all the cascade radiated modes, and not only the mode of order $k = (m - m_g)/V$. In particular, it is interesting to investigate to what extent the subcritical gusts, namely the gusts for which no cascade radiated mode k is propagating, contribute to the overall broadband noise. Firstly, a computation is done by limiting the integration to $[k_{z_{c0,\min,\text{crit.}}}, k_{z_{c0,\max,\text{crit.}}}]$, named run (*I*), depicted with symbols $\triangleright$ in Fig. 3(b). Then, three computations are performed with extended bounds $[k_{z_{c0,\min,\text{crit.}}} - \Delta k_{z_{c0}}, k_{z_{c0,\max,\text{crit.}}} + \Delta k_{z_{c0}}]$, with $\Delta k_{z_{c0}} \times c = 7$, 10 and 20 corresponding to the runs (II)–(IV) in symbols $\square$, *o* and $\times$ respectively. These simulations account for the first subcritical gusts. Three other runs are performed by imposing the cut-on criteria and requiring that the wavenumber range $[k_{z_{c0,\min}}, k_{z_{c0,\max}}]$ is at least $[-8\pi/(R_T - R_H), 8\pi/(R_T - R_H)]$ and to be at most $[-15, 15]$ for run (V) or $[-30, 30]$ for run (VI). The minimal criterion of $8\pi/(R_T - R_H)$ was previously used by Posson et al.[34,36,37] to introduce the first subcritical gusts at low frequencies while avoiding to increase the range at higher frequencies where many gusts are supercritical and where subcritical gusts are expected to have little effect. This is verified here. The value $8\pi/(R_T - R_H)$ corresponds to a cosine mode with eight nodes which has been observed to be sufficient by Atassi and Vinogradov [30] in another benchmark (noted $n_g = 4$ there). This value corresponds to $k_{z_{c0}} c \approx 7.15$ here for the NASA baseline OGV. Finally, the run (VII) accounts for all the gusts with $k_{z_{s0}} c \in [-60, 60]$. Fig. 3(a) illustrates the truncation criteria of the integral used in runs (I), (II) and (VI).

The first series of runs (I–IV) shows the important role of the subcritical gusts at low to moderate frequencies up to 6.5 kHz i.e. $k_0 R_T \approx 30$, zones (1) in Fig. 3. Indeed at 1 kHz ($k_0 R_T \approx 5$), they increase the level by 5.3 dB. However, they have negligible effect at high frequencies (zones (2)). This is quite similar to what Moreau et al. found on plane airfoils [75] and later on by Roger on an annular airfoil ring [76]. In addition, the convergence in subcritical gusts is already obtained for $\Delta k_{z_{c0}} c = 7$ at all frequencies since it perfectly agrees with run (VII). Runs (V) and (VI) are in perfect agreement below 19 kHz, whereas the run (V) underestimates the prediction above (zones (3)), because several gusts of spanwise wavenumber bigger than $k_{z_{c0}} c = 15$ are cut-on as shown in Fig. 3. At low to moderate frequencies, in range (1), the criterion $k_{z_{c0,\max}} = 8\pi/(R_T - R_H)$ is sufficient since the runs (V–VI) coincide with runs (II–IV,VII). At very low frequencies (1 kHz), the bounds of runs (V–VI) are almost equivalent to those of run (II) since there are very few supercritical gusts. At higher frequencies in zone (1), however, the criterion $k_{z_{c0,\max}} = \max(8\pi/(R_T - R_H), k_{z_{c0,\max,\text{crit.}}})$ is finer, with fewer subcritical

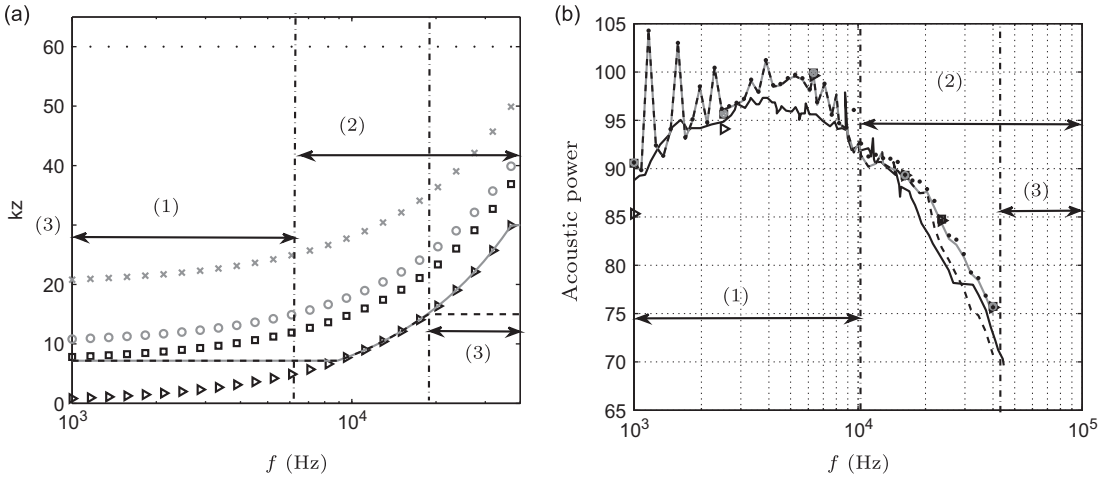

Fig. 3. NASA baseline OGV: experiment [46] (—), and present model with different bounds of the integral over the radial wavenumber $k_{z_{c0}}$: run (I) ($\triangleright$), run (II) ($\square$), run (III) ($\circ$), run (IV) ($\times$), run (V) (– – –), run (VI) (——), run (VII) ($\cdots$): (a) integral boundary $k_{z_{c0,\max}} c$ at mid-radius; (b) upstream narrow-band power spectra.

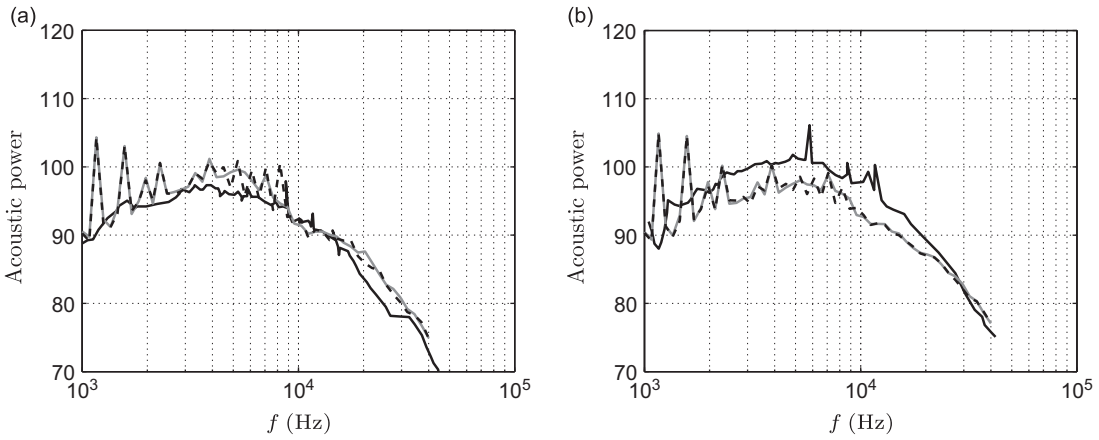

Fig. 4. NASA baseline OGV: experiment (e.g. [46]) (—), and present formulation with the cut-on criteria and $|k_{z_{R0}}c| \leq 30$ (—), with discrete value of $k_{z_{R0}}$: $k_{z_{R0}} = n\pi/(R_T - R_H)$ with n an integer ensuring the cut-on criteria and $|k_{z_{R0}}c| \leq 30$ (– – –): (a) upstream and (b) downstream narrow-band power spectra.

gusts, than the one of runs (II–IV) but it applies again. At the highest frequencies, in area (2), runs (VI) is in perfect agreement with the first series of runs and with run (VII). The subcritical gusts can then be neglected.

The radial variation of the incident turbulent field could have been written as a Fourier series instead of the present continuous Fourier transform by invoking the no-flow boundary conditions at hub and tip radii as proposed by Atassi and Vinogradov [30] in their analysis by linearized Euler equations [33]. This is questionable for turbulent velocities when the integral length scale is much smaller than the duct height. Turbulence at mid-height is not likely affected by the duct walls. However, such a formulation has the advantage of saving computational time by a factor $(R_T - R_H)/(\pi d k_{z_{R0}})$. The use of the Fourier series is found to capture the correct overall spectrum shape in Fig. 4. But it exhibits many additional peaks at intermediate frequencies between 3 and 9 kHz, which are not predicted by the continuous formulation. The peaks originate from the selection of particular wavenumbers, which emphasize resonances. From now on a continuous Fourier transform is therefore applied and the run (VI) is used as a compromise between accuracy and computational time.

3.2.2. Convergence of the series in azimuthal order of the incident perturbation m_g

As already mentioned by several authors (e.g. [32]) the number of contributing modes to the overall sound power significantly increases with the frequency. The number of Fourier components of the turbulence velocity that must be considered also rises. The truncation of the series in azimuthal order of the incident perturbation m_g must then be investigated. The sum over the azimuthal order m_g of the incident gusts is calculated by summing over the relative integers k such that $m = m_g + kB_S$. In practice, the minimal and maximal allowed values of m_g are imposed equal to $-N_{m_g}$ and N_{m_g} ($N_{m_g} = 100$, 200, 300 and 400 in Fig. 6). Then the effective limits of k are imposed by the number of values of k between $\lceil (m - N_{m_g})/B_S \rceil$ and $\lfloor (m + N_{m_g})/B_S \rfloor$. The summation over k thus over m_g reduces to a maximum of $\lceil 2N_{m_g}/B_S \rceil$ values, i.e. 8 for $m_g = 200$ and $B_S = 54$ (baseline OGV).

In addition, the rectilinear cascade defined in each strip provides two cut-on conditions, for cascade radiated mode orders: $k_{min,cascade}$ and $k_{\max,\text{cascade}}$ which are the extreme integers between the two roots of the equation

$$\omega = \omega_k = \frac{1}{s^2}[U_c d(\sigma - 2\pi k) + s_e c_0 \sqrt{(\sigma - 2\pi k)^2 + (k_{z_{c0}} s)^2}]. \tag{51}$$

These conditions are merely the translation of the previous ones on $k_{z_{c0}}$ in terms of k at fixed $k_{z_{c0}}$. They are analogous to the conditions outlined by Hanson [22] in terms of σ and $k_{z_{c0}}$ for $k = 0$ but derived here in terms of m_g and k. Finally the values of k associated with cut-on modes radiated by the cascade modes are limited in a parallelogram-like region as shown in Fig. 5 for $k_{z_{c0}} = 0$. Fig. 6 shows the effect of the bounds of the summation on the acoustic power spectra. Below 9.6 kHz ($k_0 R_T = 50$), all results collapse. The convergence in m_g is already obtained. Above this value, the results start to differ. The additional term tends to increase the response at high frequencies. Indeed, the number of modes radiated by the cascade increases with frequency. The orders of the radiated modes of the cascade equal the orders k, and the azimuthal order of the associated duct mode is $m = m_g + kB_S$ [35]. Finally, the truncation is fixed to $N_{m_g} = 200$ in the following investigation, as the numerical convergence of the integrals and series have then been reached. The origin of the peaks observed at low frequencies in the model, seen in Fig. 6 for instance, whereas the experimental spectrum is really smooth, is investigated next.

3.2.3. Resonances and spurious peaks at low frequencies

Posson and Roger [39] proposed to introduce a correction in the vicinity of the cut-on frequencies to avoid unrealistic peaks at these frequencies as briefly introduced in Section 2.6. This correction has already been applied to the above results. The effect of the correction is illustrated in Fig. 7(a). At low frequencies, it reduces the overall level by up to 10 dB,

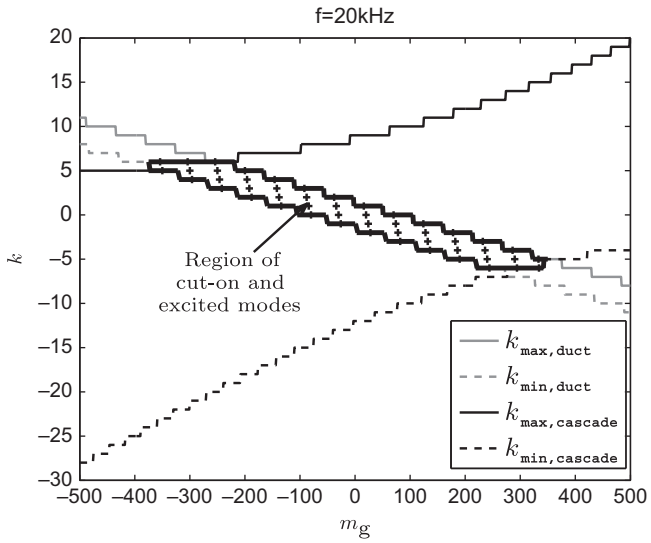

Fig. 5. NASA baseline OGV: lower and upper bounds $k_{\min,\mathrm{duct}} = \lceil(-\max(m)-m_g)/B_S\rceil$ and $k_{\max,\mathrm{duct}} = \lfloor(\max(m)-m_g)/B_S\rfloor$ of k imposed by the maximal azimuthal order m of propagating duct mode at f=20 kHz and lower and upper bounds $k_{\min,\mathrm{cascade}}$ and $k_{\max,\mathrm{cascade}}$ of k imposed by the cut-on condition of the rectilinear cascade at mid-span at f=20 kHz.

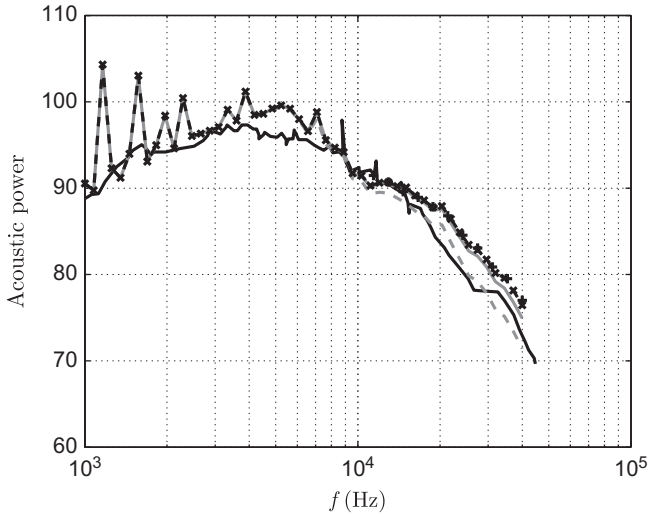

Fig. 6. Upstream narrow-band power spectra of the NASA baseline OGV: experiment [46] (—), present formulation with original blade loading, $N_{m_g} = 200$ (——), $N_{m_g} = 100$ (— — —), $N_{m_g} = 300$ (— ✕ —) and $N_{m_g} = 400$ (+).

the basis of the peaks becoming closer to the experimental results, whereas it has a negligible effect at higher frequencies where peaks are less pronounced.

However many numerical peaks remain at low frequencies. As exhibited by the different sampling of the curve in frequencies in Fig. 7(b), the low-frequency spectrum is highly contaminated by spurious peaks caused by the numerical sensitivity of the code to the low density of modes. This issue is not omitted. However to make the comparison easier, the curves obtained with 30 points over the frequency range 1–30 kHz (black dashed line in Fig. 7(b)) are used in the following sections except in Section 3.3.

3.2.4. Accuracy of the simplifications and assumptions in the acoustic power

The expression of the PSD of the acoustic power produced by a row of either rotor blades or stator vanes (Eqs. (5a), (37a), (47a)) relies on the simplification made in Sections 2.2.3 and 2.3.2 based on the existence and properties of the length L_r. The accuracy of the simplification must be assessed as a function of frequency and duct mode order. Indeed, it is valid if half the radial correlation length L_r, plotted in Fig. 8, is smaller than the radial scale of the variation of the duct mode $E_{m,\mu}$. The correlation length exhibits a hump at intermediate frequencies as shown in Fig. 8. At 25 percent of span, the hump covers a range of $k_0 R_T$ from 4 to 13 (i.e. between 0.78 and 2.52 kHz) whereas it is much wider near the tip.

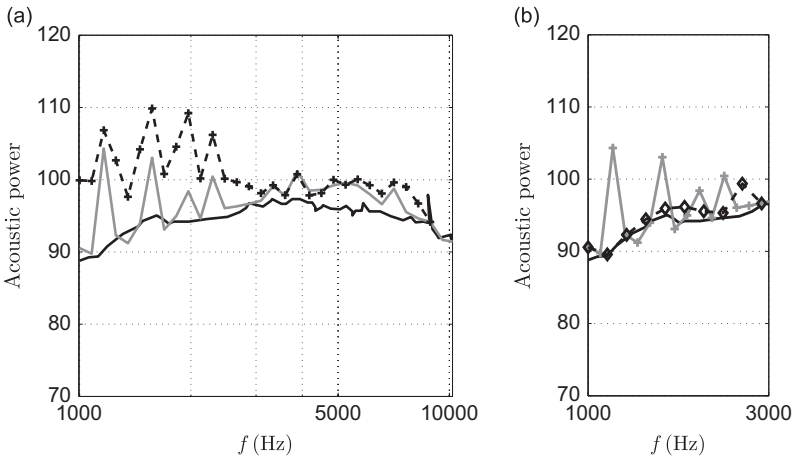

Fig. 7. NASA baseline OGV: (a) effect of the correction in the vicinity of the cut-on frequency, experimental data (—), present formulation with no correction (— + —), and with correction (——) ; (b) low-frequency spectra, experimental data (—), present formulation with 15 points in [1,3] kHz (50 up to 40 kHz) (——), and with 10 points in [1,3] kHz (30 up to 30 kHz) (— ⟡ —).

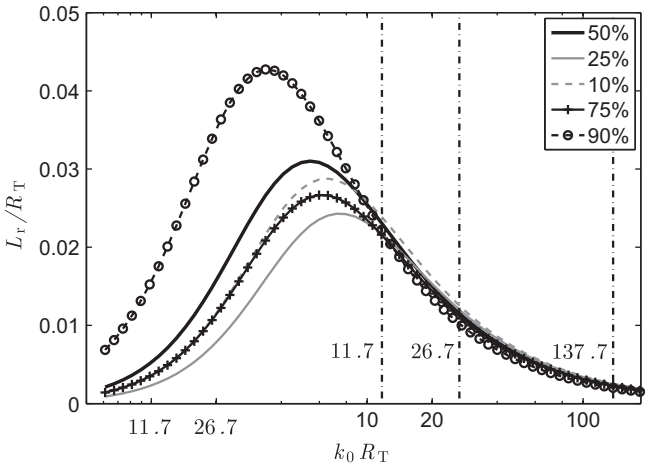

Fig. 8. NASA baseline OGV: variation of the half radial correlation length L_r with frequency at 5 radii along the span (from 10 percent to 90 percent of span) for isotropic Liepmann's model.

Another issue originates from the use of the Hankel functions in Eq. (32) instead of the Bessel functions in Eq. (3). Indeed, the Bessel function of second kind $r \mapsto Y_m(\chi_{m,\mu} r)$ goes to infinity when increasing the azimuthal order m of a duct mode with low radial order μ, in particular when $\mu = 0$. But the coefficient $B_{m,\mu} = -(J'_m(\chi_{m,\mu} R_T)/Y'_m(\chi_{m,\mu} R_T))A_{m,\mu} = -(J'_m(\chi_{m,\mu} R_H)/Y'_m(\chi_{m,\mu} R_H))A_{m,\mu}$ approaches zero with a steeper decay. Numerically, the second definition at the hub is preferred to ensure the convergence of the product $B_{m,\mu} Y_m(\chi_{m,\mu} r)$ and finally of the function $E_{m,\mu}$. The imaginary part of the Hankel functions is defined from the Bessel function of the second kind. In Eqs. (37a) and (47a), the products of the two Hankel functions with different sine cardinal functions (reminded below in Eq. (53)) may induce numerical errors. It is then required to verify the proper convergence of the formulation. For this, the expression

$$\Xi = E_{m,\mu}(r) \int_{-L_r}^{L_r} E_{m,\mu}(r+\Delta r) \mathrm{e}^{\mathrm{i}(K_\varphi - k_{z_{R_0}})\Delta r} \, \mathrm{d}\Delta r, \tag{52}$$

with $K_\varphi = k^{\pm}_{x_R,m\mu} \tan \breve{\varphi}_R - m \tan \breve{\psi}_R / r$ ($=0$ for radial vanes), is evaluated numerically and plotted in black curves in Fig. 9, for the baseline OGV, for a radial wavenumber $k_{z_{R_0}} c_S = 0$ or 20, and several frequencies and duct mode orders (m,μ). The analytical approximation:

$$2L_r[C^*_{m,\mu} H^{(1)*}_m(\chi_{m,\mu} r) \mathrm{sinc}((K_\varphi - k_{z_{R_0}} - k^*_{z_{d1}})L_r) + D^*_{m,\mu} H^{(2)*}_m(\chi_{m,\mu} r) \mathrm{sinc}((K_\varphi - k_{z_{R_0}} + k_{z_{d1}})L_r)], \tag{53}$$

obtained in Sections 2.2.3 and 2.3.2, is plotted for comparison as symbols. The solution obtained when neglecting the difference of radii in the eigenfunction $E_{m,\mu}$:

$$2L_r\left|E_{m,\mu}(r)\right|^2\mathrm{sinc}((K_\varphi - k_{z_{R_0}} + k_{z_{d1}})L_r) \tag{54}$$

is represented in grey and called *real-part approximation* later on for conciseness, simply because it results in a real number.

The plots of the quantity Ξ at $k_0R_T = 11.7$ (2.27 kHz) in Fig. 9(a), (b), (d) and (e) show a very good agreement in all cases between the numerical evaluation of the exact integral and the approximated analytical formulation. The difference of radii in the eigenfunction can be neglected (*real-part approximation*, dashed line) for a two-dimensional incident gust ($k_{z_{R0}} = 0$). For three-dimensional gusts, it is still able to predict the real part of the formulation (Fig. 9(d)), with however small discrepancies (Fig. 9(e)). Nevertheless, the imaginary part is now important and it cannot be predicted with the *real-part approximation* (Fig. 9(d) and (e)). This justifies accounting for the spanwise variation of the eigenfunction as done in the proposed analytical approximation. When increasing the frequencies to $k_0R_T = 26.7$ (5.17 kHz) (Fig. 9(c) and (f)), the conclusions are almost the same. The prediction from the analytical simplification is again very good, whereas the discrepancies of the *real-part approximation* are larger. At high frequencies ($k_0R_T = 137.7$ and f=26.68 kHz), modes of high radial orders become cut-on (e.g. $(m,\mu) = (28,23)$ in Fig. 9(g)). The radial scale of these duct modes can be rather small compared to the duct height. However, at these frequencies the radial correlation length $l_r = 2L_r$ also decreases, and finally goes to zero (Fig. 8). The assumption is still valid as shown for $k_0R_T = 137.7$ (f=26.68 kHz) in Fig. 9(g) whereas the *real-part approximation* predicts very low levels. Some discrepancies are observed for modes with small radial orders μ and high azimuthal orders m for the high spanwise wavenumber ($k_{z_{R0}}c = 20$) as in Fig. 9(h) for $(m,\mu) = (140,0)$. However, for

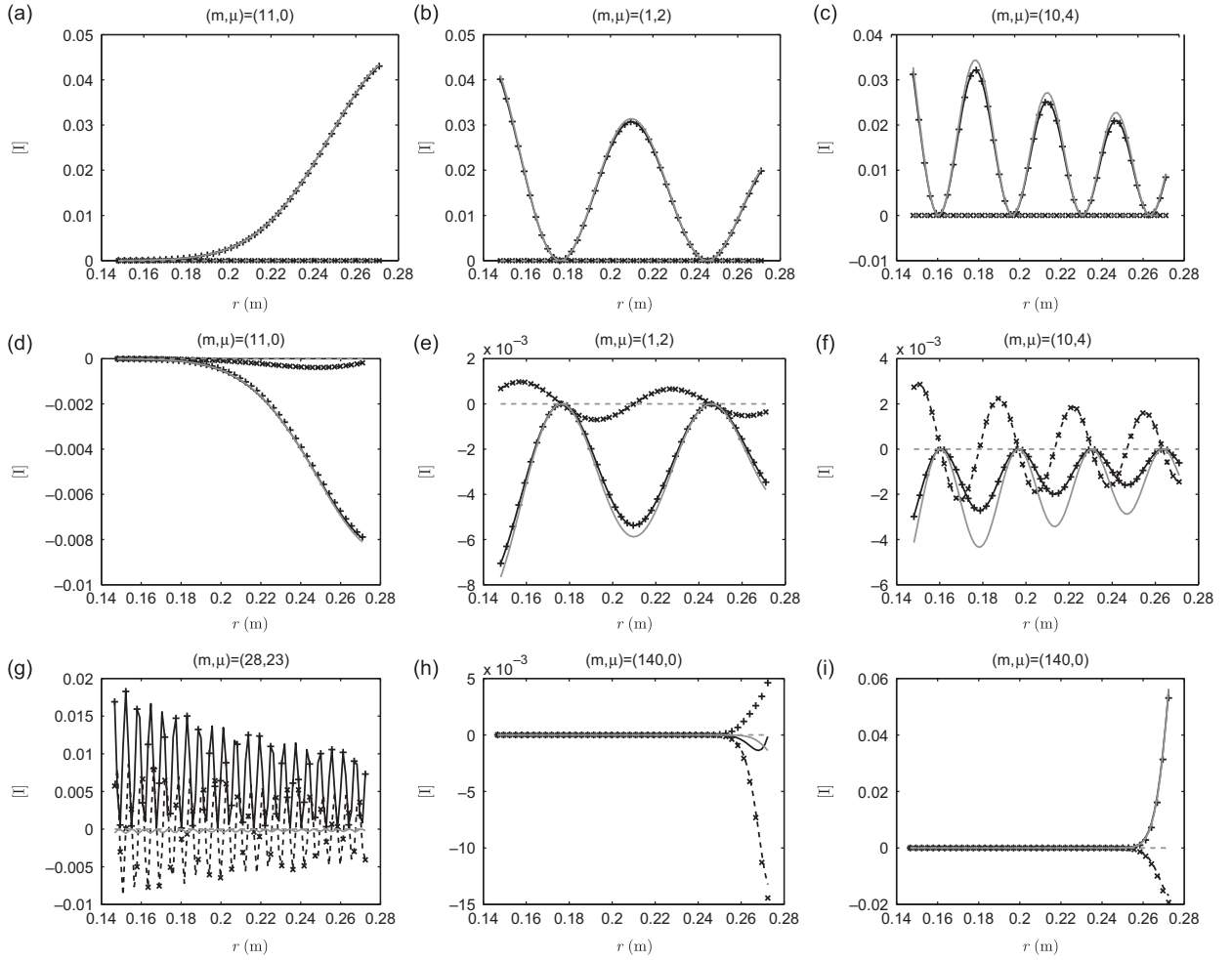

Fig. 9. Comparison of the real (— and symbols +) and imaginary (– – – and symbols ×) parts of the expression Ξ. Numerical evaluation (black), simplification of Sections 2.2.3 and 2.3.2 (symbols) and assumption $E_{m,\mu}(r+\Delta r) \approx E_{m,\mu}(r)$ (grey): (a, b) $k_0R_T = 11.7$, $k_{z_{R_0}}c_S = 0$ for (a) $(m,\mu) = (11,0)$ and (b) $(m,\mu) = (1,2)$; (d, e) $k_0R_T = 11.7$, $k_{z_{R_0}}c_S = 20$ for (d) $(m,\mu) = (11,0)$ and (e) $(m,\mu) = (1,2)$; (c,f) $k_0R_T = 26.7$ for $(m,\mu) = (10,4)$ with (c) $k_{z_{R_0}}c_S = 0$ and (f) $k_{z_{R_0}}c_S = 20$; (g–i) $k_0R_T = 137.7$ and (g) $k_{z_{R_0}}c_S = 20$ for $(m,\mu) = (28,23)$, (h) $k_{z_{R_0}}c_S = 20$ for $(m,\mu) = (140,0)$ and (i) $k_{z_{R_0}}c_S = 10$ for $(m,\mu) = (140,0)$.

moderately high values of $k_{z_{R0}}c$ (e.g. 10), no discrepancies are observed as shown in Fig. 9(i).Finally, the simplification proposed in Sections 2.2.3 and 2.3.2 performs well for the studied configurations.

3.3. Alternative formulations

The formulation of the present model (Eqs. (37a) and (47a)) referred to as (**F1**) later on, is now further simplified. Two high-frequency approximations are introduced as proposed by Posson and Roger [36]. Firstly when $k_0 L_r \gg 1$, $\mathrm{Int}(\dot{r},K_1)/(2\pi)$ can be assimilated to a Dirac delta function: $\mathrm{Int}(\dot{r},K_1) \approx (2\pi)\delta(K_i - k_{z_{I0}})$. Inserting this approximation in Eqs. (37a) and (47a) leads to the formulation referred to as (**F2**).

A final modified version resulting from the formulation (**F2**), labelled (**F3**) is proposed on the basis of the following observations. First, the wavenumbers K_i are complex and some numerical difficulties might appear, even if theoretically the formulation (**F1**) is valid if L_r can be defined and then the formulation (**F2**) should apply at high frequencies. Secondly, the rectilinear-cascade model does not produce scattering in radial wavenumbers, as pointed out in [34], and the cut-on frequencies of the cascade modes do not coincide with the cut-on frequencies of the annular duct modes [36]. A third formulation is then proposed, as suggested by Glegg [57] for the trailing-edge noise of blades in an annular duct, in order to tune the radial wavenumber $k_{z_{I0}}$ and thus $k_{z_{c0}}$ to ensure the coincidence of the wave equations and then of the cut-on frequencies. For each duct mode (m,μ), only the incident gusts with the tuned radial wavenumber contribute to the radiated field of that mode. Yet, this method artificially attributes a large contribution of this particular wavenumber near the cut-on frequencies of a duct mode. In fact, all wavenumbers of the incident turbulence contribute to the acoustic radiation of the duct mode (m,μ) and other wavenumbers cannot a priori be neglected. The new formulation must then be assessed, notably against the formulation (**F2**). Besides, this spanwise wavenumber defined for each duct mode (m,μ) corresponds to the one used in the correction in the vicinity of the cut-on frequencies (Sections 2.6 and 3.2.3) but it is used here for all frequencies and duct modes.

The results obtained with these two formulations are plotted in Fig. 10. In the upstream direction (Fig. 10(a)), the approximated formulations (**F2**) and (**F3**) are in good agreement with formulation (**F1**) above 4 kHz, the formulation (**F3**) giving even better results at the highest frequencies. (**F3**) is then relevant to tune the radial wavenumber of the gusts to ensure the coincidence of the cut-on frequencies of the cascade modes and of the duct modes. Downstream, the two formulations (**F2**) and (**F3**) predict the overall level of the experiment and the proper spectrum shape above 4 kHz well, whereas formulation (**F1**) underestimates the response. This suggests that this underestimate is introduced by the expression Ξ. However, at highest frequencies, the spectrum obtained with formulations (**F2**) and (**F3**) drops more slowly than those of the experiment and the formulation (**F1**), leading to an overestimate of about 4 dB at 30 kHz. Above all, at low frequencies, formulations (**F2**) and (**F3**) overestimate the spectrum level by up to 10–15 dB (at 1 kHz for instance), which was expected since formulations (**F2**) and (**F3**) rely on a high-frequency assumption. Finally, the corresponding strong reduction of computational time with these formulations with a moderate lack of accuracy could justify their use for parametric studies in industrial context.

3.4. Effect of the turbulence model

Liepmann's isotropic model has been used in the aforementioned predictions. Let us note that the provided data [17,42,74] for the turbulence integral length scale assumes the equality of the integral length scales $\Lambda_b(r) = \Lambda_w(r)$ of the background and wake turbulence. Turbulence properties ($u_{\mathrm{rms},i}$, Λ_i or $(l_{a,i},l_{t,i})$) define both the three-dimensional turbulence spectrum Φ_{ww} and the length l_r. The former is in factor of the cascade response and the duct mode terms

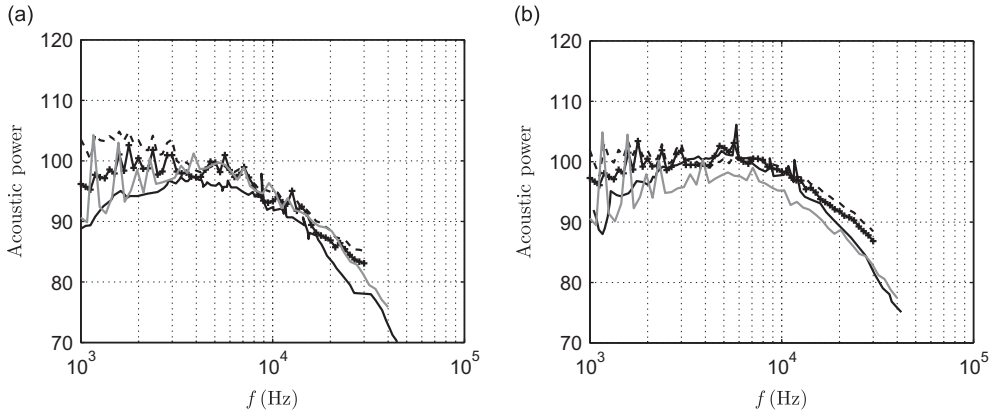

Fig. 10. NASA baseline OGV: experiment [46] (—), present formulation (**F1**) (——), simplified formulations (**F3**) (——|——), and (**F2**) (– – –): (a) upstream and (b) downstream narrow-band power spectra.

inside the integrals. It modulates the amplitudes of the gusts with different wavenumbers. The latter is involved inside and outside the sine cardinal function. It is then crucial to evaluate the effect of the turbulence model on the predicted results. First the Liepmann and the Gaussian models for isotropic turbulence are compared in Fig. 11 for the low-count OGV and are also compared with the results of Atassi and Logue [32] obtained with the LEE solver [33]. Here the corrected unsteady blade loading presented in [34] and summarized in Section 2.7 has been used for all predictions. As with the LEE solver, the use of a Gaussian spectrum produces a very steep decrease above 12 kHz. In addition, the low-frequency levels are underestimated by about 6–7 dB with the present model and of a similar amount (8 dB) with the LEE solver compared to the results with Liepmann's model. Furthermore, the model and the LEE simulation behave similarly for both turbulence models and compare favorably with the SDT cases, for which the turbulence can be considered as isotropic. Indeed, the SDT fan rig data were acquired in an ambient tunnel Mach number of 0.1 [46] which must have greatly mitigated eddies stretching during their ingestion and should be sufficient to achieve acoustic flight effect [77]. A preliminary study of the effect of turbulence anisotropy is illustrated in Fig. 12 with the axisymmetric model of Kerschen and Gliebe, for which $\Phi_{ww}(\mathbf{k}_c)$ and l_r are derived in Appendix C.2. Two different sets of parameters have been tested. The longitudinal $l_{a,i}$ and transverse $l_{t,i}$ integral length scales have been defined with respect to the turbulence intensity formerly used in the isotropic turbulence case Λ_i. Firstly, the transverse length scale has been reduced to $l_t = \Lambda/2$, while the axial length scale l_a is kept equal to Λ and $u_a = u_t = w_{rms}$. Secondly, the axial length scale l_a has been increased to $l_a = 2\Lambda$, while the transverse length scale l_t is kept equal to Λ and $u_a = u_t = w_{rms}$. The reduction of l_t only produces an unrealistic noise reduction (16 dB here) and a slight shift of the hump to lower frequencies, whereas the increase of l_a only produces a large but smaller decay at low frequencies (8 dB) and a stronger decay above 5.8 kHz. Thus, the shape of the spectrum is more distorted than with the reduction of l_t. The model is then highly sensitive to the parameters of the anisotropic model. The use of an anisotropic turbulence model is then conditioned by a proper characterization of the turbulence from experimental measurements. When this information is not available, a simpler isotropic model is more robust for noise prediction and parametric studies.

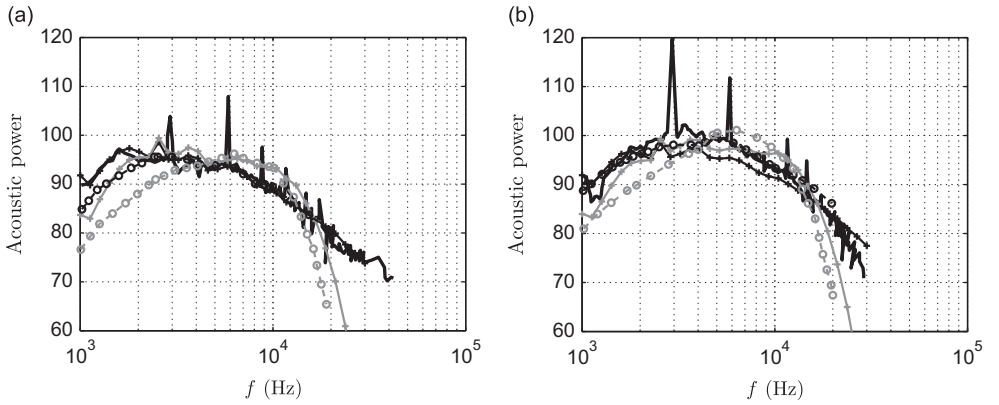

Fig. 11. NASA low-count OGV: experiment [46] (—), Atassi et al. [33] (from [32]) (— ⊖ —), present formulation with corrected unsteady blade loading (——|——). Isotropic Liepmann's model (black), and Gaussian's model (grey): (a) upstream and (b) downstream narrow-band power spectra.

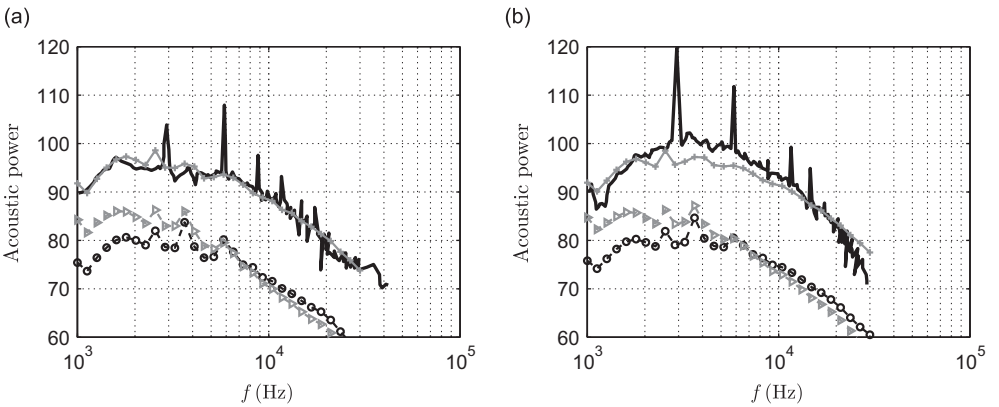

Fig. 12. NASA low-count OGV: experiment [46] (—), present formulation with Liepmann's model (——|——) and axisymmetric model for $l_t = l_a/2 = \Lambda/2$ and $u_a = u_t$ (— ⊖ —) and for $l_a = 2l_t = 2\Lambda$ and $u_a = u_t$ (— ▷ —): (a) upstream and (b) downstream narrow-band power spectra.

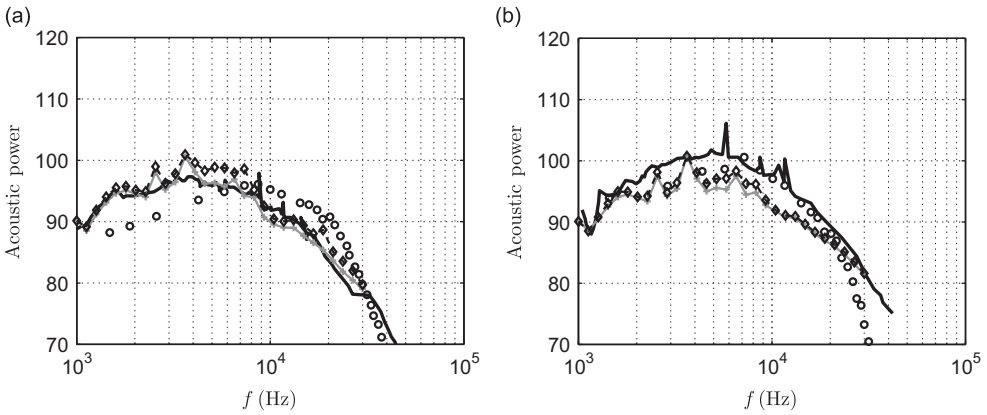

Fig. 13. NASA baseline OGV: experiment (e.g. [46]) (—), Nallasamy and Envia [17] (○), present formulation with original blade loading (——), and modified blade loading (——|——): (a) upstream and (b) downstream narrow-band power spectra.

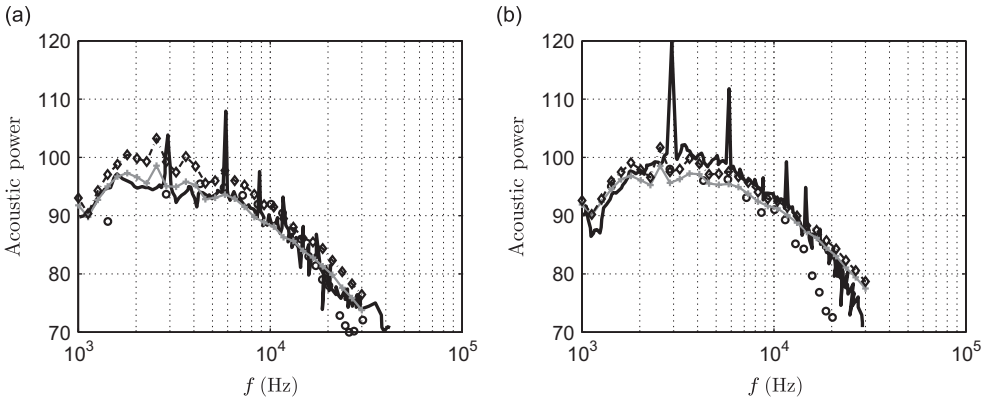

Fig. 14. NASA low-count OGV: experiment (e.g. [46]) (—), Nallasamy and Envia [17] (○), present formulation with original blade loading (— ◈ —), and modified blade loading (——|——): (a) upstream and (b) downstream narrow-band power spectra.

3.5. Final validation

Finally, the effect of the correction proposed in [34] and briefly reminded in Section 2.7 is reported in Figs. 13 and 14 for the baseline and low-count SDT test cases respectively. The correction reduces the predicted level in both configurations, with a more pronounced effect upstream of the fan (Figs. 13(a), and 14(a)) than downstream (Figs. 13(b) and 14(b)). More precisely, in the baseline configuration and upstream (Fig. 13), the correction reduces the overestimation at intermediate frequencies (2.5 dB at 5.1 kHz). At low and high frequencies, the levels remain almost unchanged. The corrected formulation then predicts the upstream acoustic power accurately whereas the downstream acoustic power remains underestimated by 3–5 dB at 5.1 kHz. The behavior is very similar in the low-count OGV case (Fig. 14), for which the correction significantly improves the prediction over the whole frequency range. The upstream acoustic power is again in very good agreement with the experiment. The downstream acoustic power is underestimated by 3 dB. The present model compares better with the experiment than the model developed by Nallasamy and Envia in all four cases, except at mid-frequency in the downstream direction for the baseline case. At high frequencies, this is mainly attributed to the choice of Liepmann's model. At other frequencies, the corrected three-dimensional response recently developed by Posson et al. [34,35] is the main reason. At low frequencies, the contribution of the subcritical gusts accounted for in the present model is also significant.

4. Concluding remarks

An analytical model for predicting the broadband noise produced by the interaction of ingested turbulence with the rotor blades of a fan and the rotor-wake impingement on outlet guide vanes has been described in detail. The model resorts to a strip-theory approach and an unsteady blade-loading rectilinear-cascade response [35] extending Glegg's analytical formulation [21]. The model has been extensively compared with experimental results of the 22-in source diagnostic test (SDT) fan rig of the NASA Glenn Research Center, which is a very realistic turbomachinery configuration

involving the rotor–stator interaction-noise mechanism. Possible simplifications of the model have been thoroughly assessed in order to reduce the computation time. Indeed the analytical formulations involve integrals and sums. The truncation of the integral over the spanwise wavenumbers of the incident turbulent gusts has been investigated. The subcritical gusts are shown to be necessary at low frequencies to capture the correct level, whereas the supercritical gusts underestimate the radiation by 5 dB. A convergence in subcritical gusts is also proved. In the NASA baseline case, it is ensured by accounting for the subcritical gusts with non-dimensional spanwise wavenumbers apart by less than 7 from the spanwise-wavenumbers range of supercritical gusts. At higher frequencies subcritical gusts have negligible effects as previously shown on airfoils [75,76]. The effect of turbulence modelling has also been studied. Turbulence in the SDT cases is almost homogeneous and isotropic in some radial layers. The prediction with Liepmann's model gives the best results. The Gaussian isotropic spectrum leads to a too strong decay at the highest frequencies and an underestimate of 6–7 dB at low frequencies, which is consistent with Atassi and Logue's results [32]. The expressions of the turbulence properties required by the model for Kerschen and Gliebe's axisymmetric turbulence model have also been derived. A first result with a reduction by a factor 2 of the transverse length scale l_t of a half shows a strong noise level reduction of about 14 dB, for instance. The present preliminary results underline the strong effect of turbulence modelling. Finally, the correction of the unsteady blade loading proposed in a previous work by the authors [34] has been shown to provide a better prediction of the upstream acoustic power. However the present model still underestimates the downstream acoustic power by 2–5 dB. Finally, two further approximations have been proposed from the original model at high frequencies. These formulations are in rather good agreement with the experiment above 4 kHz. Their faster computational time makes them useful for parametric studies in an industrial context.

Acknowledgments

The authors wish to acknowledge Dr. Edmane Envia from NASA Glenn Research Center for providing the overall geometric and aerodynamic data of the NASA 22-in fan source diagnostic test. They also acknowledge Compute Canada and the RQCHP (Quebec, Canada) for providing computational resources.

Appendix A. Reference frames, coordinate transformation and geometrical parameters

A.1. Reference frames, coordinate transformation

The coordinates $\mathbf{X}|_d$, $\mathbf{X}|_I$, $\mathbf{X}|_{cd}$, $\mathbf{X}|_c$ in the different frames of reference $\mathcal{R}_d$, $\mathcal{R}_I$, $\mathcal{R}_{cd}$, $\mathcal{R}_c$ respectively are linked by

$$\mathbf{X}|_I = \begin{pmatrix} x_I \\ y_I \\ r \end{pmatrix} = \begin{pmatrix} x_d \\ y_d \\ r \end{pmatrix} - \begin{pmatrix} 0 \\ -\Omega_I r t \\ 0 \end{pmatrix}, \tag{A.1}$$

$$\mathbf{X}|_{cd} = \begin{pmatrix} x_{cd} \\ y_{cd} \\ z_{cd} \end{pmatrix} = \mathbf{Q}_{\breve{\chi}\psi,I} \bullet \begin{pmatrix} x_I - x_{\mathrm{LE},I}(r) \\ y_I - y_{\mathrm{LE},I}(r) \\ 0 \end{pmatrix}, \tag{A.2}$$

$$\mathbf{X}|_c = \begin{pmatrix} x_c \\ y_c \\ z_c \end{pmatrix} = \mathbf{Q}_{\varphi,I} \bullet \mathbf{X}|_{cd} = \mathbf{Q}_{\breve{\chi}\psi\varphi,I} \bullet \begin{pmatrix} x_I - x_{\mathrm{LE},I}(r) \\ y_I - y_{\mathrm{LE},I}(r) \\ 0 \end{pmatrix}, \tag{A.3}$$

where $x_{\mathrm{LE},I}(r)$ and $y_{\mathrm{LE},I}(r)$ are the positions of the leading-edge of the blade 0 at the radius r along $\mathbf{e}_{x,I}$ and $\mathbf{e}_{y,I}$. They are defined by the relation (A.4) and they introduce phase shifts because of the sweep $\breve{\varphi}_I$ and the lean $\breve{\psi}_I$ of the blades:

$$\begin{cases} x_{\mathrm{LE},I}(r) = (r - R_H)\sin\breve{\varphi}_I, \\ y_{\mathrm{LE},I}(r) = (r - R_H)\sin\breve{\psi}_I. \end{cases} \tag{A.4}$$

The transformation matrices $\mathbf{Q}_{\breve{\chi}\psi,I}$ and $\mathbf{Q}_{\breve{\chi}\psi\varphi,I}$ defined by Eqs. (A.5) and (A.6) are rotation matrices that rotate the frames of reference linked to the duct axis to the frames of reference linked to the cascade axis around a particular radius. The first matrix is a rotation of the stagger angle $\breve{\chi}_I$ followed by a rotation of the lean angle (after stagger) ψ_I. The second matrix corresponds to the same transformation followed by a rotation of the sweep angle (after stagger and lean angles) φ_I:

$$\mathbf{Q}_{\breve{\chi}\psi,I} = \begin{pmatrix} \cos\breve{\chi}_I & \sin\breve{\chi}_I & 0 \\ -\sin\breve{\chi}_I\cos\psi_I & \cos\breve{\chi}_I\cos\psi_I & -\sin\psi_I \\ -\sin\breve{\chi}_I\sin\psi_I & \cos\breve{\chi}_I\sin\psi_I & \cos\psi_I \end{pmatrix}, \tag{A.5}$$

$$\mathbf{Q}_{\check{\chi}\psi\varphi,I}=\begin{pmatrix}\cos\check{\chi}_I\cos\varphi_I+\sin\check{\chi}_I\sin\psi_I\sin\varphi_I & \sin\check{\chi}_I\cos\varphi_I-\cos\check{\chi}_I\sin\psi_I\sin\varphi_I & -\cos\psi_I\sin\varphi_I\\ -\sin\check{\chi}_I\cos\psi_I & \cos\check{\chi}_I\cos\psi_I & -\sin\psi_I\\ \cos\check{\chi}_I\sin\varphi_I-\sin\check{\chi}_I\sin\psi_I\cos\varphi_I & \sin\check{\chi}_I\sin\varphi_I+\cos\check{\chi}_I\sin\psi_I\cos\varphi_I & \cos\psi_I\cos\varphi_I\end{pmatrix}, \tag{A.6}$$

and

$$\mathbf{Q}_{\check{\chi}\psi\varphi,I}=\mathbf{Q}_{\varphi,I}\mathbf{Q}_{\check{\chi}\psi,I}=\mathbf{Q}_{\varphi,I}\mathbf{Q}_{\psi,I}\mathbf{Q}_{\check{\chi},I} \tag{A.7}$$

with

$$\mathbf{Q}_{\varphi,I}=\begin{pmatrix}\cos\varphi_I & 0 & -\sin\varphi_I\\ 0 & 1 & 0\\ \sin\varphi_I & 0 & \cos\varphi_I\end{pmatrix}. \tag{A.8}$$

The matrix of the inverse transformation $Q_{\mathrm{inv},I}=Q^{-1}_{\check{\chi}\psi\varphi,I}$ is equal to

$$\mathbf{Q}_{\mathrm{inv},I}=\begin{pmatrix}\cos\check{\chi}_I\cos\varphi_I+\sin\check{\chi}_I\sin\psi_I\sin\varphi_I & -\sin\check{\chi}_I\cos\psi_I & \cos\check{\chi}_I\sin\varphi_I-\sin\check{\chi}_I\sin\psi_I\sin\varphi_I\\ \sin\check{\chi}_I\cos\varphi_I-\cos\check{\chi}_I\sin\psi_I\sin\varphi_I & \cos\check{\chi}_I\cos\psi_I & \sin\check{\chi}_I\sin\varphi_I+\cos\check{\chi}_I\sin\psi_I\cos\varphi_I\\ -\cos\psi_I\sin\varphi_I & -\sin\psi_I & \cos\psi_I\cos\varphi_I\end{pmatrix}. \tag{A.9}$$

The lean and sweep angles ψ_I, φ_I are related to the lean angle looking from the front of the duct $\check{\psi}_I$ and the sweep angle looking from the side $\check{\varphi}_I$ as detailed by [22] and reminded here:

$$\begin{cases}\tan\psi_I=\cos\check{\chi}_I\tan\check{\psi}_I-\sin\check{\chi}_I\tan\check{\varphi}_I,\\ \tan\varphi_I=\cos\psi_I(\sin\check{\chi}_I\tan\check{\psi}_I+\cos\check{\chi}_I\tan\check{\varphi}_I).\end{cases} \tag{A.10}$$

Finally the stagger angle of the rectilinear-cascade model χ_I is defined by

$$\tan\chi=\frac{\mathbf{Q}_{\check{\chi}\psi\varphi,I,12}}{\mathbf{Q}_{\check{\chi}\psi\varphi,I,22}}. \tag{A.11}$$

An additional reference frame $\tilde{\mathcal{R}}_I$, whose $\tilde{x}$-axis is along $\boldsymbol{\lambda}$ and the $\tilde{z}$-axis is radial, is introduced in Appendix C.2 to deal with axisymmetric turbulence. The transformation matrix from this reference frame to the cascade reference frame $\mathcal{R}_c$, $\tilde{\mathbf{Q}}_I$, is

$$\tilde{\mathbf{Q}}_I=\begin{pmatrix}\cos\Delta\check{\chi}_I\cos\tilde{\varphi}_I+\sin\Delta\check{\chi}_I\sin\tilde{\psi}_I\sin\tilde{\varphi}_I & \sin\Delta\check{\chi}_I\cos\tilde{\varphi}_I-\cos\Delta\check{\chi}_I\sin\tilde{\psi}_I\sin\tilde{\varphi}_I & -\cos\tilde{\psi}_I\sin\tilde{\varphi}_I\\ -\sin\Delta\check{\chi}_I\cos\tilde{\psi}_I & \cos\Delta\check{\chi}_I\cos\tilde{\psi}_I & -\sin\tilde{\psi}_I\\ \cos\Delta\check{\chi}_I\sin\tilde{\varphi}_I-\sin\Delta\check{\chi}_I\sin\tilde{\psi}_I\cos\tilde{\varphi}_I & \sin\Delta\check{\chi}_I\sin\tilde{\varphi}_I+\cos\Delta\check{\chi}_I\sin\tilde{\psi}_I\cos\tilde{\varphi}_I & \cos\tilde{\psi}_I\cos\tilde{\varphi}_I\end{pmatrix}, \tag{A.12a}$$

with

$$\begin{cases}\tan\tilde{\psi}_I=\cos\Delta\check{\chi}_I\tan\check{\psi}_I-\sin\Delta\check{\chi}_I\tan\check{\varphi}_I,\\ \tan\tilde{\varphi}_I=\cos\tilde{\psi}_I(\sin\Delta\check{\chi}_I\tan\check{\psi}_I+\cos\Delta\check{\chi}_I\tan\check{\varphi}_I).\end{cases} \tag{A.12b}$$

It simply differs from $\mathbf{Q}_I$ by replacing the stagger angle $\check{\chi}_I$ by $\Delta\check{\chi}_I$.

A.2. Relationship between velocities

The triangle of velocities and the cascade angles impose the following relationships between the mean velocity components.

A.2.1. Relationship between velocities in the rotor case

$$\tan\check{\chi}_R=\frac{\Omega_R r}{U_{x_d}},\quad U_0=\frac{U_{x_d}}{\cos\check{\chi}_R},$$

$$U_c=U_0\cos\varphi_R,\quad W_c=U_0\sin\varphi_R. \tag{A.13}$$

A.2.2. Relationship between velocities in the stator case

$$U_0=\frac{U_{x_d}}{\cos\check{\chi}_S},\quad U_\theta=U_{x_d}\tan\check{\chi}_S$$

$$U_c=U_0\cos\varphi_S,\quad W_c=U_0\sin\varphi_S,$$

$$\Omega_R r=U_{x_d}(\tan\check{\chi}_S-\tan\check{\chi}_R),\quad U_y=U_{x_d}\tan\check{\chi}_R. \tag{A.14}$$

Appendix B. Cascade parameters

g is the inter-blade distance, that is to say the distance between two leading edges in a section of the duct. Several parameters of the rectilinear-cascade model are introduced in the equations. They have been originally defined by [21] and recalled by [35]. They are given here for the sake of completeness:

$$d = Q_{\check{\chi}\psi\varphi,12} g_I, \quad h = Q_{\check{\chi}\psi\varphi,22} g_I, \quad s = \sqrt{d^2+h^2}$$

$$M = U_c/c_0, \quad \beta^2 = 1-M^2, \quad s_e = \sqrt{d^2+\beta^2 h^2}$$

$$M_w = W_c/c_0, \quad \beta_w^2 = 1-M_w^2. \tag{B.1}$$

d and h are the stagger distance and the inter-blade distance normal to the blade in the cascade frame of reference $\mathcal{R}_c$. M is the Mach number along the blade in the chordwise direction:

$$Mh = M_{xd} s, \quad s_e = \beta_{xd} s \tag{B.2}$$

Appendix C. Turbulence models

C.1. Isotropic turbulence model

Liepmann's model can be used to model a locally isotropic homogeneous turbulence. In Cartesian coordinates, the turbulence spectrum $\Phi_{ww} = \Phi_{2,2}$ in the cascade frame of reference $\mathcal{R}_c$ divided by the turbulence intensity is defined as

$$\Phi_{ww}^{\text{Liep}}(\mathbf{k}_c) = \frac{2\Lambda^5}{\pi^2} \frac{k_{x_c}^2 + k_{z_c}^2}{(1+\Lambda^2 k_s^2)^3} \tag{C.1}$$

with $k_s^2 = k_{x_c}^2 + k_{y_c}^2 + k_{z_c}^2$, and the radial correlation length l_r is given by

$$l_r \equiv l_r^{\text{Liep}}(\omega) = \frac{3\pi\Lambda}{2\sqrt{1+(K_x\Lambda)^2}} \frac{(K_x\Lambda)^2}{1+3(K_x\Lambda)^2}. \tag{C.2}$$

A Gaussian isotropic model can also be used [32]. The turbulence longitudinal correlation coefficient is assumed to be: $f(x) = \exp(-\pi x^2/(4\Lambda^2))$, leading to the three-dimensional energy spectrum $E(k\Lambda) = 4u_{\text{rms}}^2 k_s \Lambda^5 \exp(-(k_s\Lambda)^2/\pi)/\pi^3$. The turbulence spectrum Φ_{ww} and the radial correlation length l_r can then be derived:

$$\Phi_{ww}^{\text{Gauss}}(\mathbf{k}_c) = \frac{\Lambda^5}{\pi^4} \mathrm{e}^{-(k_s\lambda)^2/\pi} [k_{x_c}^2 + k_{z_c}^2], \quad l_r^{\text{Gauss}}(\omega) = \frac{(K_x\Lambda)^2\Lambda}{\frac{\pi}{2}+(K_x\Lambda)^2}. \tag{C.3}$$

C.2. Axisymmetric turbulence model

Following Kerschen and Gliebe's work [62], the dimensional three-dimensional cross-spectrum of the i and j components of the turbulence velocity is defined by

$$\Phi_{ij}(\mathbf{k}) = [k^2\delta_{i,j} - k_i k_j]\mathcal{F} + [(k^2 - (\mathbf{k}\cdot\boldsymbol{\lambda})^2)\delta_{i,j} - k_i k_j - k^2\lambda_i\lambda_j + \mathbf{k}\cdot\boldsymbol{\lambda}(\lambda_i k_j + \lambda_j k_i)]\mathcal{G}, \tag{C.4}$$

where

$$\mathcal{F} = \frac{F_0}{(1+l_a^2 k_a^2 + l_t^2 k_t^2)^3}, \quad F_0 = \frac{2u_a^2 l_a l_t^4}{\pi^2}, \quad \mathcal{G} = \mathcal{B}\mathcal{F} \quad \text{and} \quad \mathcal{B} = \frac{2u_t^2}{u_a^2} - \frac{l_t^2}{l_a^2} - 1, \tag{C.5}$$

and $\boldsymbol{\lambda}$ is the unit vector in the direction of the symmetry. The wavenumber is k_a in the direction of symmetry and k_{ty} and k_{tz} in the transverse directions with $k_t = \sqrt{k_{ty}^2 + k_{tz}^2}$. u_a and u_t are the root mean square values of the fluctuating velocities in the direction of the axis of symmetry and in the transverse direction respectively. l_a and l_t are similarly the integral length scales of the turbulence in the direction of the axis of symmetry and in transverse direction. The only constraint is that

$$2\frac{u_t^2}{u_a^2} \geq \frac{l_t^2}{l_a^2}. \tag{C.6}$$

Using the relation between the turbulence energy spectrum $E(k)$ and the three-dimensional turbulence spectrum

$$E(k) = \frac{1}{2} \iiint_{\mathbb{R}^3} \sum_{i=1}^{3} \tilde{\Phi}_{ii}(\boldsymbol{k}) \delta(\|\boldsymbol{k}\| - k)\, \mathrm{d}\boldsymbol{k} \tag{C.7}$$

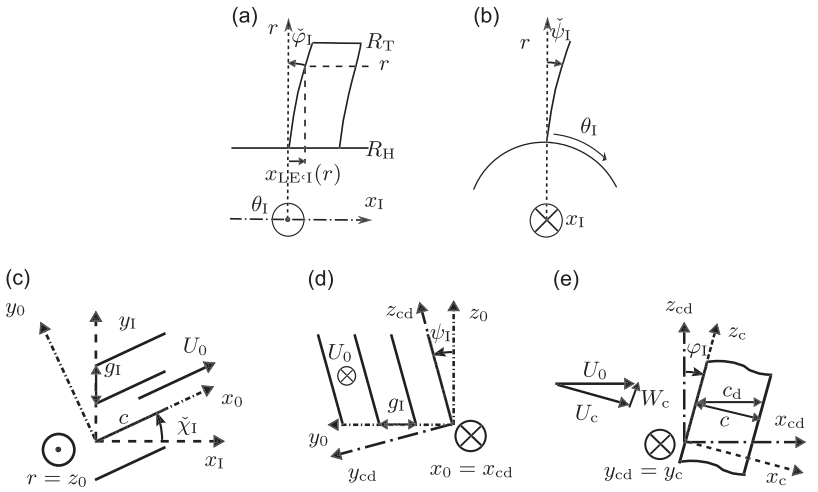

Fig. C1. Definition of the rotation angles of the cascade with the successive frames of references: (a) cascade sweep angle $\breve{\varphi}_I$ looking from the side view (fixed θ_I); (b) cascade lean angle $\breve{\psi}_I$ looking from the front view (fixed x_I); (c) cascade stagger angle $\breve{\chi}_I$ looking from an unwrapped cascade view at constant radius r; (d) cascade lean angle ψ_I after rotation of stagger angle $\breve{\chi}_I$; (e) cascade sweep angle φ_I after rotation of stagger angle $\breve{\chi}_I$ and lean angle $\breve{\psi}_I$. $\breve{\varphi}_I$, $\breve{\psi}_I$ and $\breve{\chi}_I$ are the angles given by the aerodynamic design of the row.

(see for instance [78, p. 219]), and the formulae (C.17), it can be verified that the three-dimensional turbulence spectrum of Kerschen and Gliebe satisfies as required:

$$E(k) = \tfrac{1}{2}[u_a^2 + 2u_t^2]. \tag{C.8}$$

As suggested by Hanson [22], the turbulence symmetry axis $\boldsymbol{\lambda}$ is assumed to be aligned with the flow in stationary coordinates. Namely, for a rotor impinged by ingested turbulence $\boldsymbol{\lambda} = \mathbf{e}_{x_d}$ and for a stator $\boldsymbol{\lambda} = \mathbf{e}_{x_0}$ where $\mathbf{e}_{x_0}$ is obtained by rotating $\mathbf{e}_{x_d}$ of the stagger angle $\breve{\chi}_S$ around the rotational axis $\mathbf{e}_{z_d} = \mathbf{e}_r$ (Fig. C1(c)). Let us define the reference frame $\tilde{\mathcal{R}}_I$ of associated Cartesian coordinates $(\tilde{x}_I, \tilde{y}_I, \tilde{z}_I)$, whose $\tilde{x}_I$-axis is along $\boldsymbol{\lambda}$ and the $\tilde{z}_I$-axis is radial. The transformation matrix from this reference frame to the cascade reference frame $\mathcal{R}_c$, $\tilde{\mathbf{Q}}_I$, is given in Eq. (A.12a) in Appendix A.1. It is obtained from the transformation matrix $\mathbf{Q}_I$ (between $\mathcal{R}_I$ and $\mathcal{R}_c$) simply by replacing the stagger angle $\breve{\chi}_I$ by $\Delta\breve{\chi}_I$ with $\Delta\breve{\chi}_R = \langle \boldsymbol{\lambda}, \mathbf{e}_{x_0} \rangle = \breve{\chi}_R$ in the rotor case and $\Delta\breve{\chi}_R = \breve{\chi}_S = 0$ in the stator case. As a result, the direction of the axis of symmetry is

$$\boldsymbol{\lambda} = (1,0,0)|_{\sim} = (\tilde{Q}_{11}, \tilde{Q}_{21}, \tilde{Q}_{31})|_c. \tag{C.9}$$

The wavenumbers k_a, k_{ty} and k_{tz} then become

$$\begin{aligned} k_a &= \tilde{Q}_{11}k_{x_{c0}} + \tilde{Q}_{21}k_{y_{c0}} + \tilde{Q}_{31}k_{z_{c0}}, \\ k_{ty} &= \tilde{Q}_{12}k_{x_{c0}} + \tilde{Q}_{22}k_{y_{c0}} + \tilde{Q}_{32}k_{z_{c0}}, \\ k_{tz} &= \tilde{Q}_{13}k_{x_{c0}} + \tilde{Q}_{23}k_{y_{c0}} + \tilde{Q}_{33}k_{z_{c0}} \end{aligned} \tag{C.10}$$

as given by Hanson.

Since the interesting direction for the current problem is the upwash direction y_c, the spectrum is given in the cascade frame of reference $\mathcal{R}_c$ as a function of the cascade wavenumber $\mathbf{k}_c$. After some algebra and factorization, the three-dimensional spectrum of the axisymmetric turbulence reads

$$\Phi_{ww}(\mathbf{k}_c) = [k_{x_c}^2 + k_{z_c}^2 + \mathcal{B}(\tilde{Q}_{31}k_{x_c} - \tilde{Q}_{11}k_{z_c})^2]\mathcal{F}. \tag{C.11}$$

When the radial correlation length l_r is calculated, the expressions

$$\widehat{\Phi}_{ww}(K_x, 0) = \int_{\mathbb{R}} \Phi_{ww}(K_x, k_{y_c}, 0)\, \mathrm{d}k_{y_c}, \tag{C.12}$$

with $K_x = \omega/U_s$ ($U_s = U_{x_d}$ for the rotor and $U_s = U_0$ for the stator), and

$$\breve{\Phi}_{ww}(\omega) = \iiint_{\mathbb{R}^3} \Phi_{ww}(\mathbf{k}_c)\delta(\omega - k_{x_c}U_0)\, \mathrm{d}\mathbf{k}_c \tag{C.13}$$

are not derived from Eq. (C.11) to avoid cumbersome integrand expressions, since, for instance, k_{y_c} is found in k_a, k_{ty} and k_{tz}. Instead, the following relations are used:

$$\Phi_{ww} = \tilde{Q}_{21}^2\Phi_{11} + 2\tilde{Q}_{21}\tilde{Q}_{22}\Phi_{12} + 2\tilde{Q}_{21}\tilde{Q}_{23}\Phi_{13} + \tilde{Q}_{22}^2\Phi_{22} + 2\tilde{Q}_{22}\tilde{Q}_{23}\Phi_{23} + \tilde{Q}_{23}^2\Phi_{33}, \tag{C.14}$$

and by linearity of the integral operators:

$$\widehat{\Phi}_{ww}(K_x,0)=\tilde{Q}_{21}^2\widehat{\Phi}_{11}(K_x,0)+2\tilde{Q}_{21}\tilde{Q}_{22}\widehat{\Phi}_{12}(K_x,0)+2\tilde{Q}_{21}\tilde{Q}_{23}\widehat{\Phi}_{13}(K_x,0)+\tilde{Q}_{22}^2\widehat{\Phi}_{22}(K_x,0)+2\tilde{Q}_{22}\tilde{Q}_{23}\widehat{\Phi}_{23}(K_x,0)+\tilde{Q}_{23}^2\widehat{\Phi}_{33}(K_x,0), \tag{C.15}$$

and

$$\check{\Phi}_{ww}(\omega)=\tilde{Q}_{21}^2\check{\Phi}_{11}(\omega)+2\tilde{Q}_{21}\tilde{Q}_{22}\check{\Phi}_{12}(\omega)+2\tilde{Q}_{21}\tilde{Q}_{23}\check{\Phi}_{13}(\omega)+\tilde{Q}_{22}^2\check{\Phi}_{22}(\omega)+2\tilde{Q}_{22}\tilde{Q}_{23}\check{\Phi}_{23}(\omega)+\tilde{Q}_{23}^2\check{\Phi}_{33}(\omega), \tag{C.16}$$

where Φ_{ij}, $\widehat{\Phi}_{ij}(K_x,0)$ and $\check{\Phi}_{ij}(\omega)$ are expressed in the reference frame $\tilde{\mathcal{R}}$. $\widehat{\Phi}_{ij}(K_x,0)$ and $\check{\Phi}_{ij}(\omega)$ are derived for each (i,j). The integrals are computed using the formula [79, Eq.3.241 (4)]:

$$\int_0^\infty \frac{u^{\mu-1}\mathrm{d}u}{(p+qu^\nu)^{n+1}}=\frac{1}{\nu p^{n+1}}\left(\frac{p}{q}\right)^{\mu/\nu}\frac{\Gamma\left(\frac{\mu}{\nu}\right)\Gamma\left(n+1-\frac{\mu}{\nu}\right)}{\Gamma(n+1)},\quad \forall 0<\frac{\mu}{\nu}<n+1. \tag{C.17}$$

This leads to

$$\widehat{\Phi}_{ww}(K_x,0)=\frac{\pi F_0}{8D^{5/2}l_t^3}[(\tilde{Q}_{21}^2+\tilde{Q}_{23}^2(1+\mathcal{B}))D+3(K_xl_t)^2(1-\tilde{Q}_{21}^2)] \tag{C.18}$$

and

$$\check{\Phi}_{ww}(\omega)=\frac{\pi F_0}{4U_sl_t^4D^2}[2(K_x^2l_t^2)+(1+\mathcal{B})D-\tilde{Q}_{21}^2(2(K_x^2l_t^2)+(\mathcal{B}-1)D)], \tag{C.19}$$

with $D=1+K_x^2l_a^2$. Finally, using Eqs. (48), (C.18) and (C.19), the radial correlation length is equal to

$$l_r=\frac{\pi l_t}{2D^{1/2}}\frac{3(K_xl_t)^2+\tilde{Q}_{21}^2[D-3(K_xl_t)^2]+\tilde{Q}_{23}^2[1+\mathcal{B}]D}{[1+\mathcal{B}]D+2(K_xl_t)^2-\tilde{Q}_{21}^2[(\mathcal{B}-1)D+2(K_xl_t)^2]} \tag{C.20}$$

In the case of the stator with zero lean and sweep $\tilde{Q}_{21}=\tilde{Q}_{23}=0$, in addition if $u_t=u_a$ and $l_t=l_a$, the spectrum and the radial correlation length yield the previous expressions given by Liepmann's isotropic model.

References

[1] B.D. Mugridge, C.L. Morfey, Sources of noise in axial flow fans, *Journal of the Acoustical Society of America* 51 (5, part I) (1971) 1411–1426.
[2] R. Mani, Noise due to interaction of inlet turbulence with isolated stators and rotors, *Journal of Sound and Vibration* 17 (2) (1971) 251–260.
[3] D.B. Hanson, Unified analysis of fan stator noise, *Journal of the Acoustical Society of America* 54 (6) (1973) 1571–1591.
[4] Sevik, Sound radiation from a subsonic rotor subjected to turbulence, *In its Fluid Mechanics, Acoustics, and Design of Turbomachinery, Part II*, NASA Sp-304, Pennsylvania State University, University Park, 1974, pp. 493–512.
[5] G.F. Homicz, A.R. George, Broadband and discrete frequency radiation from subsonic rotors, *Journal of Sound and Vibration* 36 (1974) 151–177.
[6] A.R. George, Y.N. Kim, High frequency broadband rotor noise, *AIAA Journal* 15 (4) (1977) 538–545 also AIAA Paper 76-561.
[7] R.K. Amiet, Noise produced by turbulent flow into propeller or helicopter rotor, *AIAA Journal* 15 (3) (1977) 307–308 also AIAA Paper 76-560.
[8] N.A. Cumpsty, Review—a critical review of turbomachinery noise, *Journal of Fluids Engineering, Transaction of ASME* 99 (1977) 278–293.
[9] T.F. Brooks, R.H. Schlinker, Progress in rotor broadband noise research, *Vertica (ISSN 0360-5450)* 4 (1983) 287–307.
[10] A.R. George, S.T. Chou, Comparison of broadband noise mechanisms, analyses, and experiments on rotors, *Journal of Aircraft* 21 (3797) (1984) 583–592.
[11] S.A.L. Glegg, Broadband noise from ducted prop fans, *15th Aeroacoustics Conference*, Long Beach, CA, no. AIAA Paper 1993-4402, 1993, pp. 1–14.
[12] B. De Gouville, Calcul du bruit à large bande d'un rotor caréné dû à la turbulence incidente. Application aux soufflantes de turboréacteurs (Computation of the Broadband Noise Produced by the Interaction of Ingested Turbulence with a Ducted Rotor. Application to the Turbofans.), PhD Thesis, Ecole Centrale de Lyon, n° ordre : 98-39, Septembre 1998.
[13] P. Joseph, A. Parry, Rotor/wall boundary-layer interaction broadband noise in turbofan engines, *7th AIAA/CEAS Aeroacoustics Conference and Exhibit*, Maastricht, Netherlands, no. AIAA Paper 2001-2244, 2001, pp. 1–11.
[14] J.M.R. Graham, Similarity rules for thin aerofoils in non-stationary subsonic flows, *Journal of Fluid Mechanics* 43 (4) (1970) 753–766.
[15] E. Envia, D.L. Tweedt, R.P. Woodward, D.M. Elliott, E.B. Fite, C.E. Hughes, G.G. Podboy, D.L. Sutliff, An assessment of current fan noise prediction capability, *14th AIAA/CEAS Aeroacoustics Conference and Exhibit*, Vancouver, Canada, no. AIAA Paper 2008-2991, 2008, pp. 1–46.
[16] C.S. Ventres, M.A. Theobald, W.D. Mark, Turbofan Noise Generation, Volume 1: Analysis, Contractor Report CR-167952, NASA, 1982.
[17] M. Nallasamy, E. Envia, Computation of rotor wake turbulence noise, *Journal of Sound and Vibration* 282 (2005) 649–678.
[18] U.W. Ganz, P.D. Joppa, T.J. Patten, D.F. Scharpf, Boeing 18-inch Fan Rig Broadband Noise Test, Contractor Report CR-1998-208704, NASA, 1998.
[19] D.B. Hanson, Quantification of inflow turbulence for prediction of cascade broadband noise, *Specialist Keynote Paper, Fifth International Congress on Sound and Vibration*, Adelaide, South Australia, 1997, pp. 515–529.
[20] D.B. Hanson, K.P. Horan, Turbulence/cascade interaction: spectra of inflow, cascade response, and noise, *4th AIAA/CEAS Aeroacoustics Conference and Exhibit*, Toulouse, France, no. AIAA Paper 1998-2319, 1998, pp. 688–700.
[21] S.A.L. Glegg, The response of a swept blade row to a three-dimensional gust, *Journal of Sound and Vibration* 227 (1) (1999) 29–64.
[22] D.B. Hanson, Theory of Broadband Noise for Rotor and Stator Cascade with Inhomogeneous Inflow Turbulence Including Effects of Lean and Sweep, Contractor Report CR-210762, NASA, 2001.
[23] D.B. Hanson, Broadband Noise of Fans. With Unsteady Coupling Theory to Account for Rotor and Stator Reflection/Transmission Effects, Contractor Report CR-211136-REV1, NASA, 2001.
[24] S.A.L. Glegg, Broadband Fan Noise Generated by Small Scale Turbulence, Contractor Report CR-207752, NASA, 1998.
[25] S.A.L. Glegg, N. Walker, Fan noise from blades moving through boundary layer turbulence, *5th AIAA/CEAS Aeroacoustics Conference and Exhibit*, Bellevue, WA, no. AIAA Paper 1999-1888, 1999.
[26] I. Evers, N. Peake, On sound generation by the interaction between turbulence and a cascade of airfoils with non-uniform mean flow, *Journal of Fluid Mechanics* 463 (2002) 25–52.
[27] C. Cheong, P. Joseph, L. Soogab, High-frequency formulation for the acoustic power spectrum due to cascade-turbulence interaction, *Journal of the Acoustical Society of America* 119 (1) (2006) 108–122.

[28] S.N. Smith, Discrete frequency sound generation in axial flow turbomachines, Aeronautical Research Council Reports and Memoranda 3709, 1973, pp. 1–59.
[29] V. Jurdic, A. Moreau, P. Joseph, L. Enghardt, C.J., A comparison between measured and predicted fan broadband noise due to rotor-stator interaction, *13th AIAA/CEAS Aeroacoustics Conference and Exhibit*, Rome, Italy, no. AIAA Paper 2007-3692, 2007, pp. 1–16.
[30] H.M. Atassi, I.V. Vinogradov, A model for fan broadband interaction noise in nonuniform flow, *11th AIAA/CEAS Aeroacoustics Conference and Exhibit*, Monterey, CA, no. AIAA Paper 2005-2880, 2005, pp. 1–12.
[31] H.M. Atassi, I.V. Vinogradov, Modelling broadband fan noise and comparison with experiments, *13th AIAA/CEAS Aeroacoustics Conference and Exhibit*, Rome, Italy, no. AIAA Paper 2007-3691, 2007, pp. 1–13.
[32] H.M. Atassi, M.M. Logue, Effect of turbulence structure on broadband fan noise, *14th AIAA/CEAS Aeroacoustics Conference and Exhibit*, Vancouver, Canada, no. AIAA Paper 2008-2842, 2008, pp. 1–14.
[33] H.M. Atassi, A.A. Ali, O.V. Atassi, I.V. Vinogradov, Scattering of incidence disturbances by an annular cascade in a swirling flow, *Journal of Fluid Mechanics* 499 (2004) 111–138.
[34] H. Posson, S. Moreau, M. Roger, On the use of a uniformly valid analytical cascade response function for broadband noise predictions, *Journal of Sound and Vibration* 329 (18) (2010) 3721–3743.
[35] H. Posson, M. Roger, S. Moreau, Upon a uniformly valid analytical rectilinear cascade response function, *Journal of Fluid Mechanics* 663 (2010) 22–52.
[36] H. Posson, M. Roger, Experimental validation of a cascade response function for fan broadband noise predictions, *14th AIAA/CEAS Aeroacoustics Conference and Exhibit*, Vancouver, BC, Canada, no. AIAA Paper 2008-2844, 2008, pp. 1–20.
[37] H. Posson, S. Moreau, M. Roger, Fan-OGV broadband noise prediction using a cascade response, *15th AIAA/CEAS Aeroacoustics Conference and Exhibit*, Miami, FL, no. AIAA Paper 2009-3150, 2009, pp. 1–18.
[38] H.M. Atassi, G. Hamad, Sound generated in a cascade by three-dimensional disturbances convected in subsonic flow, *7th AIAA Aeroacoustics Conference*, Palo Alto, CA, no. AIAA Paper 1981-2046, 1981, pp. 1–13.
[39] H. Posson, M. Roger, Experimental validation of a cascade response function for fan broadband noise predictions, *AIAA Journal*, in press.
[40] E. Envia, Fan noise source diagnostic test—vane unsteady pressure results, *8th AIAA/CEAS Aeroacoustics Conference and Exhibit*, Breckenridge, CO, no. AIAA Paper 2002-2430 and NASA TM-2002-211808, 2002.
[41] L.J. Heidelberg, Fan noise source diagnostic test—tone modal structure results, *8th AIAA/CEAS Aeroacoustics Conference and Exhibit*, Breckenridge, CO, no. AIAA Paper 2002-2428 and NASA TM-2002-211594, 2002.
[42] C.E. Hughes, Aerodynamic performance of scale-model turbofan outlet guide vanes designed for low-noise, *8th AIAA/CEAS Aeroacoustics Conference and Exhibit*, Breckenridge, CO, no. AIAA Paper 2002-0374/NASA/TM-2001-211352, 2002.
[43] C.E. Hughes, R.J. Jeracki, R.P. Woodward, C.J. Miller, Fan noise source diagnostic test—rotor alone aerodynamic performance results, *8th AIAA/CEAS Aeroacoustics Conference and Exhibit*, Breckenridge, CO, no. AIAA Paper 2002-2426, 2002.
[44] G.G. Podboy, M.J. Krupar, S.M. Helland, C.E. Hughes, Steady and unsteady flow field measurements within a NASA 22 inch fan model, *8th AIAA/CEAS Aeroacoustics Conference and Exhibit*, Breckenridge, CO, no. AIAA Paper 2002-1033 and NASA/TM-2003-212319, 2002.
[45] G.G. Podboy, M.J. Krupar, C.E. Hughes, R.P. Woodward, Fan noise source diagnostic test—LDV measured flow field results, *8th AIAA/CEAS Aeroacoustics Conference and Exhibit*, Breckenridge, CO, no. AIAA Paper 2002-2431 and NASA/TM-2003-212330, 2002.
[46] R.P. Woodward, C.E. Hughes, R.J. Jeracki, C.J. Miller, Fan noise source diagnostic test—far-field acoustic results, *8th AIAA/CEAS Aeroacoustics Conference and Exhibit*, Breckenridge, CO, no. AIAA Paper 2002-2427 and NASA TM-2002-211591, 2002.
[47] V.V. Golubev, H.M. Atassi, A. Lipatov, 3-D unsteady effects in annular cascades with swirl and comparison with 2D-strip theory, *3rd AIAA/CEAS Aeroacoustics Conference and Exhibit*, Atlanta, GA, no. AIAA Paper 97-1634-CP, 1997, pp. 400–410.
[48] B. Elhadidi, H.M. Atassi, Acoustic and hydrodynamic response of an annular cascade to inflow disturbances in swirling flows, *Proceedings of FEDSM3, 4th ASME/JSME Joint Fluid Engineering Conference*, July 6–11, 2003, Honolulu, Hawaii, USA, FEDSM2003 (45410), 2003, pp. 1–11.
[49] B.L. Morin, Broadband noise prediction system for gas turbine engines, *5th AIAA/CEAS Aeroacoustics Conference and Exhibit*, Bellevue, WA, no. AIAA Paper 99-1889, 1999.
[50] B.L. Morin, Broadband Fan Noise Prediction System for Turbofan Engines. Volume 3: BFANS Validation and Test Cases, Contractor Report CR-2010-216898/Vol3, 2010.
[51] M.E. Goldstein, *Aeroacoustics*, McGraw-Hill, New York, 1976.
[52] V.V. Golubev, H.M. Atassi, Unsteady swirling flows in annular cascades, Part 1: evolution of incident disturbance, *AIAA Journal* 38 (7) (2000) 1142–1149.
[53] V.V. Golubev, H.M. Atassi, Unsteady swirling flows in annular cascades, Part 2: aerodynamic blade response incident disturbance, *AIAA Journal* 38 (7) (2000) 1150–1158.
[54] C.J. Heaton, N. Peake, Algebraic and exponential instability of inviscid swirling flow, *Journal of Fluid Mechanics* 565 (2006) 279–318.
[55] J.C. Hardin, D. Huff, C.K. Tam, Benchmark problems, in: M.D.N.G.R.C. Dahl (Ed.), *Third Computational Aeroacoustics (CAA) Workshop on Benchmark Problems*, no. NASA Conference Publication 2000-209790, 2000, pp. 1–22.
[56] J.M. Tyler, T.G. Sofrin, Axial flow field of an axial compressor noise studies, *SAE Transactions* 70 (1962) 309–332.
[57] S.A.L. Glegg, C. Jochault, Broadband self-noise from a ducted fan, *AIAA Journal* 36 (8) (1998) 1387–1395.
[58] L. Soulat, S. Moreau, H. Posson, Wake model effects on the prediction of turbulence-interaction broadband noise in a realistic compressor stage, *41st AIAA Fluid Dynamics Conference and Exhibit*, Honolulu, HA, no. AIAA Paper 2011-3900, 2011.
[59] R.K. Amiet, Acoustic radiation from an airfoil in a turbulent stream, *Journal of Sound and Vibration* 41 (1975) 407–420.
[60] J.O. Hinze, *Turbulence*, McGraw Hill, New York, 1959.
[61] H.W. Liepmann, J. Laufer, L.K., On the Spectrum of Isotropic Turbulence, Technical note 2473, National Advisory Committee for Aeronautics, California Institute of Technology, November 1951.
[62] E.J. Kerschen, P.R. Gliebe, Noise caused by the interaction of a rotor with anisotropic turbulence, *AIAA Journal* 19 (6) (1981) 717–723.
[63] D.B. Hanson, Spectrum of rotor noise caused by atmospheric turbulence, *Journal of the Acoustical Society of America* 56 (1) (1974) 110–126.
[64] G.K. Batchelor, The theory of axisymmetric turbulence, *Proceedings of the Royal Society of London. Series A, Mathematical and Physical Sciences* 186 (1007) (1946) 480–502.
[65] S. Chandrasekhar, The theory of axisymmetric turbulence, *Philosophical Transactions of the Royal Society of London, Series A* 242 (1950) 557–577.
[66] S. Chandrasekhar, The decay of axisymmetric turbulence, *Proceedings of the Royal Society of London. Series A, Mathematical and Physical Sciences* 203 (1950) 358–364.
[67] R. Mani, Isolated Rotor Noise due to Inlet Distortion or Turbulence, Technical Report, NASA, October 1974.
[68] R. Mani, K. Bekofske, Experimental and Theoretical Studies of Subsonic Fan Noise, Technical Report, NASA, March 1976.
[69] H.S. Ribner, M. Tucker, Spectrum of Turbulence in a Contracting Stream, NACA Report 1113, NACA, 1953.
[70] G.K. Batchelor, I. Proudman, The effect of rapid distortion of a fluid in turbulent motion, *The Quarterly Journal of Mechanics and Applied Mathematics* 7 (1954) 83–103.
[71] H.M. Atassi, M.M. Logue, Fan broadband noise in anisotropic turbulence, *15th AIAA/CEAS Aeroacoustics Conference and Exhibit*, Miami, FL, USA, no. AIAA Paper 2009-3148, 2009, pp. 1–11.
[72] K.H. Hall, Exact solution to category 3 problems—turbomachinery noise, C.K.W. Tam, J.C. Hardin (Eds.), *Second Computational Aeroacoustics (CAA) Workshop on Benchmark Problems*, vol. 3352, NASA Conference Publication1997, pp. 41–43.
[73] H. Posson, S. Moreau, R. Roger, Classical wake/stator interactions addressed with an analytical cascade model, *Canadian Aeronautics and Space Institute AERO'09 Conference Aerodynamics Symposium*, Ottawa, BC, 2009, pp. 1–9.

[74] E. Envia, private communication, NASA Glenn Research Center, Cleveland, OH, USA, March 2009.
[75] S. Moreau, M. Roger, Effect of angle of attack and airfoil shape on turbulence-interaction noise, *11th AIAA/CEAS Aeroacoustics Conference and Exhibit*, Monterey, CA, no. AIAA Paper 2005-2973, 2005, pp. 1–20.
[76] M. Roger, On broadband jet-ring interaction noise and aerofoil turbulence-interaction noise predictions, *Journal of Fluid Mechanics* 653 (2010) 337–364.
[77] D. Chestnutt, Flight Effects of Fan Noise, Technical Report NASA CP-2242, NASA, January 1982.
[78] S.B. Pope, *Turbulent Flows*, Cambridge University Press, 2000.
[79] I.S. Gradshteyn, I.M. Ryzhik, *Tables of Integrals, Series, and Products*, Academic Press, New York, 1980.